

Bosonization and DMRG study of FFLO phase and irrational magnetization plateaus in coupled chains

G. Roux,^{1,*} E. Orignac,^{2,†} P. Pujol,¹ and D. Poilblanc¹

¹*CNRS UMR 5152 - Laboratoire de Physique Théorique, Université de Toulouse,
118 Route de Narbonne, 31062 Toulouse, France.*

²*CNRS UMR 5672 - Laboratoire de Physique de l'Ecole Normale Supérieure de Lyon,
46, Allée d'Italie, 69007 Lyon, France*
(Dated: October 13, 2019)

We review the properties of two coupled fermionic chains, or ladders, under a magnetic field parallel to the lattice plane. Results are computed by complementary analytical (bosonization) and numerical (density-matrix renormalization group) methods which allows a systematic comparison. Limiting cases such as coupled bands and coupled chains regimes are discussed. We particularly focus on the evolution of the superconducting correlations under increasing field and on the presence of irrational magnetization plateaus. We found the existence of large doping-dependent magnetization plateaus in the weakly-interacting and strong-coupling limits and in the non-trivial case of isotropic couplings. We report on the existence of extended Fulde-Ferrell-Larkin-Ovchinnikov phases within the isotropic t-J and Hubbard models, deduced from the evolution of different observables under magnetic field. Emphasis is put on the variety of superconducting order parameters present at high magnetic field. We have also computed the evolution of the Luttinger exponent corresponding to the ungaped spin mode appearing at finite magnetization. In the coupled chain regime, the possibility of having polarized triplet pairing under high field is predicted by bosonization.

PACS numbers: 71.10.Pm, 74.20.Mn, 74.81.-g, 75.40.Mg

I. INTRODUCTION

Low-dimensional strongly correlated systems have attracted strong interest in the last years because fluctuations and energetic competitions drive these systems into exotic phases. Quasi-one dimensional or strongly anisotropic two dimensional systems are also known to be good candidates for the realization of Fulde-Ferrell-Larkin-Ovchinnikov (FFLO) phases^{1,2}. Qualitatively, the FFLO mechanism consists in giving singlet Cooper pairs a finite momentum (thus breaking translational symmetry) which leads to an inhomogeneous superconducting order parameter. In a singlet superconductor under high magnetic fields, there is a competition between polarizing the spin of electrons and binding them into Cooper pairs leading to a theoretical critical field called Pauli limit or paramagnetic limit^{2,3}. But, this limit can be exceeded with an inhomogeneous order parameter (FFLO) which can be energetically favorable, allowing pockets of polarized electrons and paired electrons. Among the intriguing low-dimensional systems, ladders, which consist of a few coupled chains, proved to display deep new physical behaviors and sustained considerable experimental and theoretical work⁴.

At half filling, ladders are Mott insulators and have a spin gap if the number of chains is even (this gap goes to zero in the limit of infinite number of coupled chains) and no spin gap if it is odd. The two-leg ladder has thus a spin-liquid ground state with exponentially decaying magnetic correlations. Spin gaps can also open under magnetic field for rational values of the magnetization per site leading to plateaus in the magnetization curve⁵. Experimental evidences of zero magneti-

zation plateaus have been reported on ladder and coupled dimers compounds^{6,7,8} such as $\text{Cu}_2(\text{C}_5\text{H}_{12}\text{N}_2)_2\text{Cl}_4$, $(\text{C}_5\text{H}_{12}\text{N})_2\text{CuBr}_4$ and $(5\text{IAP})_2\text{CuBr}_4 \cdot 2\text{H}_2\text{O}$. Away from half-filling, a few systems are known to develop irrational magnetization plateaus controlled by hole concentration^{9,10,11}. Furthermore, when holes are introduced into the spin-liquid two-leg ladder, these charge carriers generically bring the system into either a metallic or a superconducting state. The isotropic two-leg ladder is known to have a wide superconducting phase^{12,13} and also a metallic phase with dominant charge density waves¹⁴ (CDW). Another interesting effect is the appearance of commensurate CDW for a commensurate hole concentration¹⁴. The theoretically proposed framework to account for superconductivity relies on magnetic fluctuations and is based on the Resonating-Valence-Bond (RVB) mechanism for superconductivity proposed by Anderson in the context of high- T_c superconductors¹⁵. Within the isotropic Hubbard and t-J models, singlet pairing with an unconventional modified d -wave structure is found. The competition¹⁶ between superconductivity and CDW has indeed been observed in the cuprate ladder compound $\text{Sr}_{14-x}\text{Ca}_x\text{Cu}_{24}\text{O}_{41+\delta}$ (SCCO) for which the superconducting state only appears under high pressure¹⁷. However, the mechanism responsible for superconductivity in SCCO has not reached a full agreement yet. In this context, the upper critical magnetic fields determined from transport measurements^{18,19} suggest that the Pauli limit is exceeded in SCCO which reassesses the issue of the nature of the pairing. Note that superconductivity has also been discovered in the zig-zag ladder subsystem of the cuprate compound $\text{Pr}_2\text{Ba}_4\text{Cu}_7\text{O}_{15-\delta}$ at ambient pressure²⁰.

Recently, a two-leg t-J ladder under a strong magnetic field in the plane of the ladder was studied numerically²¹ using the Density-Matrix Renormalization Group^{22,23} (DMRG) method. The magnetic curve displays a doping-dependent magnetization plateau, as predicted²⁴ by Cabra *et al.* for a Hubbard ladder. In addition to this non-trivial magnetic behavior, an exceeding of the Pauli limit was found. Within the t-J model, this exceeding was explained by a one-dimensional analogue of the FFLO phase, hence reconciling the expectation of singlet pairing and the exceeding of the Pauli limit. Lastly, the behavior of the superconducting correlations studied in Ref. [21] showed a non-trivial behavior in and outside the plateau.

In this article, we propose to extend previous results by comparing bosonization and numerical calculations to understand the physics underlying various situations. While most studies on the FFLO phase resort to mean-field theories for low-dimensional and unconventional superconductors, we here use these two approaches which are more suited to quasi one-dimensional strongly-correlated systems. In the same spirit, an early study on the superconducting phase of the t-J chain which gave evidence of developing FFLO-like correlations²⁵ was based on exact diagonalization computations, and bosonization has also been used on an attractive Hubbard system in this context²⁶.

The article is organized as follow: first, after introducing microscopic models (Sec. II), we briefly examine the non-interacting and strong-coupling limits in Sec. III where large doping-dependent magnetization plateaus can occur. The coupled bands regime is discussed in details in Sec. IV and corresponds to the case of doped isotropic ladders which is the most studied at zero magnetic field. Lastly, the coupled chains regime is studied under magnetic field (Sec. V).

II. MICROSCOPIC MODELS AND CONVENTION

We describe the ladder system with a standard one-orbital Hubbard model which can have different hopping terms along the chains (\parallel) and between the chains (\perp). We consider a situation where no magnetic orbital effect is present and thus only keep a Zeeman coupling to the spin degree of freedom. This would experimentally correspond to the situation where the magnetic field H is in the plane of the ladder (and even along the direction of the ladder to minimize all orbital effects). Then, one can

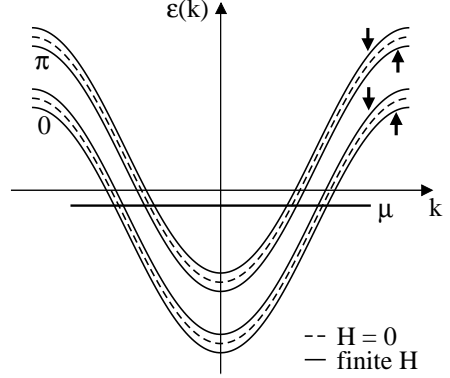


FIG. 1: Splitting of the bands dispersion in a non-interacting doped ladder (μ is the chemical potential) due to Zeeman effect at low magnetic field H .

write the Hubbard Hamiltonian

$$\begin{aligned} \mathcal{H} = & -t_{\parallel} \sum_{i,p=1,2,\sigma} [c_{i+1,p,\sigma}^{\dagger} c_{i,p,\sigma} + h.c.] \\ & -t_{\perp} \sum_{i,\sigma} [c_{i,2,\sigma}^{\dagger} c_{i,1,\sigma} + h.c.] \\ & + U \sum_{i,p=1,2} n_{i,p,\uparrow} n_{i,p,\downarrow} \\ & - \sum_{i,p=1,2} H \cdot \mathbf{S}_{i,p} \end{aligned} \quad (1)$$

where $c_{i,p,\sigma}^{\dagger}$, $\mathbf{S}_{i,p}$ and $n_{i,p,\sigma}$ are respectively electron creation, spin and density operators at site i on chain p and σ is the spin index. The $g\mu_B$ prefactor has been absorbed in the definition of H for convenience. Free bands dispersion is given by

$$\varepsilon_{k_y,\sigma}(k) = -2t_{\parallel} \cos(k) - t_{\perp} \cos(k_y) - H \frac{\sigma}{2} \quad (2)$$

(with $k = k_x$ for simplicity and $k_y = 0, \pi$) and are sketched in FIG. 1. If we denote by k_{F,k_y}^{σ} the Fermi wave-vectors, we have the Luttinger sum rule

$$n = \frac{1}{2\pi} \sum_{(k_y,\sigma) \text{ occ.}} k_{F,k_y}^{\sigma}, \quad (3)$$

where $n = N^e/(2L) = 1 - \delta$ is the electron density and δ the hole density and L the length of the ladder. Experimentally, cuprate systems have a fixed hole doping δ rather than a fixed chemical potential μ so δ will be kept fixed in this article. Similarly, the magnetization per site $m = (N^{\uparrow} - N^{\downarrow})/(2L)$ satisfies

$$m = \frac{1}{2\pi} \sum_{(k_y,\sigma) \text{ occ.}} \sigma k_{F,k_y}^{\sigma}. \quad (4)$$

Relations (3) and (4) are also valid in the presence of interactions. Note that Yamanaka-Oshikawa-Affleck²⁷ criteria (YOA) takes the simple form $1 - \delta \pm m \in \mathbb{Z}$ for doped

two-leg ladders. In the strong-coupling limit $U \gg t$ and for small hole doping, Hamiltonian (1) reduces to the t-J model:

$$\begin{aligned} \mathcal{H} = & -t_{\parallel} \sum_{i,p=1,2,\sigma} \mathcal{P}[c_{i+1,p,\sigma}^{\dagger} c_{i,p,\sigma} + h.c.] \mathcal{P} \\ & -t_{\perp} \sum_{i,\sigma} \mathcal{P}[c_{i,2,\sigma}^{\dagger} c_{i,1,\sigma} + h.c.] \mathcal{P} \\ & + J_{\parallel} \sum_{i,p=1,2} [\mathbf{S}_{i,p} \cdot \mathbf{S}_{i+1,p} - \frac{1}{4} n_{i,p} n_{i+1,p}] \\ & + J_{\perp} \sum_i [\mathbf{S}_{i,1} \cdot \mathbf{S}_{i,2} - \frac{1}{4} n_{i,1} n_{i,2}] \\ & - \sum_{i,p=1,2} \mathbf{H} \cdot \mathbf{S}_{i,p}, \end{aligned} \quad (5)$$

in which \mathcal{P} is the Gutzwiller projector, $n_{i,p} = \sum_{\sigma} n_{i,p,\sigma}$ and the same convention is used to label the antiferromagnetic couplings $J_{\parallel,\perp} = 4t_{\parallel,\perp}^2/U$. In what follows, these two microscopic models will be studied numerically and the isotropic model will assume $t = t_{\parallel} = t_{\perp}$ and $J = J_{\parallel} = J_{\perp}$.

Bosonization allows to study the low-energy properties and correlation functions of 1D-like systems using field theoretical methods. The bosonization Hamiltonians used to describe ladders^{28,29,30,31,32} fall into two classes, coupled bands models to be reviewed in Sec. IV and coupled chains models to be reviewed in Sec. V. The first approach is more appropriate to study the system with isotropic parameters. There is however the possibility, by strongly reducing the interchain hopping amplitude t_{\perp} , to obtain a cross-over to a regime where the coupled chain model is best suited to describe the behavior of the system (Sec. V).

III. NON-INTERACTING AND STRONG-COUPLING LIMITS

Non-interacting system. It is interesting to discuss first the non-interacting system using the relations (2) and keeping δ fixed instead of the chemical potential. Two main cases are possible: either a strong interband coupling with $t_{\perp} > 2t_{\parallel}$ or a small interband coupling for $t_{\perp} < 2t_{\parallel}$.

In the first case, the only bands which are partially filled at low magnetic field are the up and down spins bonding bands $(0,\uparrow)$ and $(0,\downarrow)$ (see FIG. 2 (a)). A first critical field corresponds to the complete filling of $(0,\uparrow)$ (FIG. 2 (b)). This induces a plateau with $m = \delta$ in the magnetization curve. This plateau is doping-dependent and similar to what has been predicted for other doped systems^{10,11}. The width of the plateau can be deduced from energetic considerations¹¹ to be $2(t_{\perp} - 2t_{\parallel})$ in our case. When the plateau ends (FIG. 2 (c)), the band (π,\uparrow) starts to be partially filled. When the band $(0,\downarrow)$ gets empty, all electrons are polarized and the magnetization curve is constant with value $m = 1 - \delta$. For open

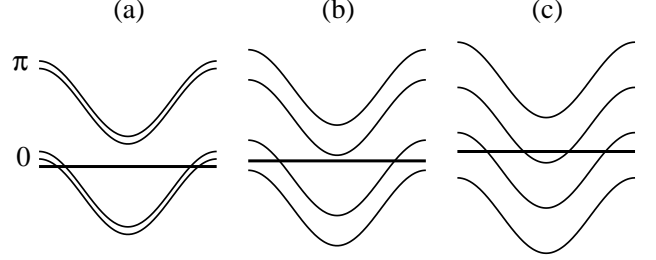


FIG. 2: Bands evolution corresponding to FIG. 3.

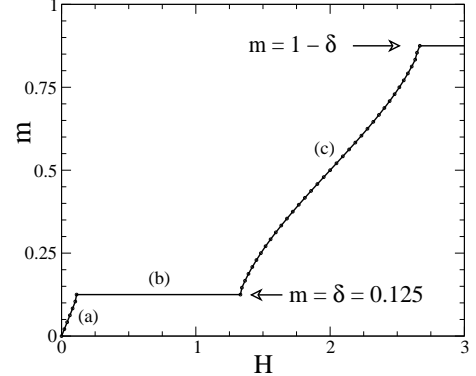


FIG. 3: Magnetization curves for the free system with $t_{\parallel} = 0.2$ and $t_{\perp} = 1.0$ showing a plateau at $m = \delta$ of width $2(t_{\perp} - 2t_{\parallel})$.

boundary conditions (OBC), a $m = \delta$ plateau is also found as displayed in FIG. 3 (see Sec. IVE 1 for computational details). The width is in good agreement with $2(t_{\perp} - 2t_{\parallel})$. Note that this plateau does not originate from interactions contrary to what will be discussed in the strong-coupling approach below and in Sec. IVE 1, but is simply due to band-filling effects.

In the second case, all four bands are partially filled at low magnetic field. No plateaus are found but filling or emptying successively the bands will induce cusps in the magnetization curve and a decrease of the slope of the magnetization because fewer electrons contribute to the magnetization. First, the band (π,\uparrow) gets empty, next $(0,\uparrow)$ becomes completely filled and lastly, $(0,\downarrow)$ gets empty corresponding to the saturation of the magnetization. An example of such a curve for $t_{\parallel} = t_{\perp}$ with OBC is given on FIG. 16. Two cusps are visible in this curve as well as a decrease of the average slope of the magnetization.

Qualitative remarks on the strong-coupling limit. Adding interactions in the system offers the possibility to study magnetization plateaus due to interactions and also pairing, which does not necessarily mean superconductivity. In this limit we have $J_{\parallel}, t_{\parallel}, t_{\perp} \ll J_{\perp}$ and the pairing energy defined as in Eq. (33) is estimated to be³³ $J_{\perp} - 2t_{\perp} - 2t_{\parallel}$ and remains approximately constant under magnetic field because the average magnetization in Eq. (33) is zero. Two ground states are possible at finite magnetization: either holes are paired up and all the polarization is due to triplets, or holes pairs are split apart

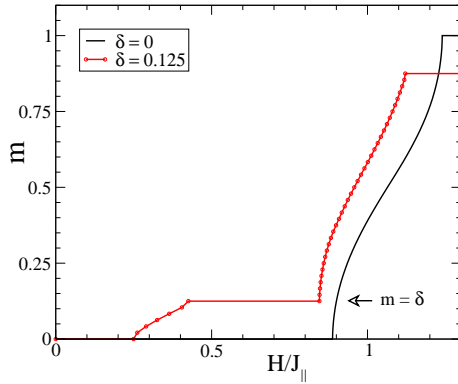


FIG. 4: (Color online) Plateaus in the strong-coupling limit. We chose $J_{\perp} = 2.5$, $J_{\parallel} = 0.3$ and $t_{\perp} = t_{\parallel} = 1.0$. The $m = \delta$ plateau is an effect of interactions and the ground-state in this plateau has unpaired holes. Still, holes are paired for magnetizations with $m \leq m_c < \delta$.

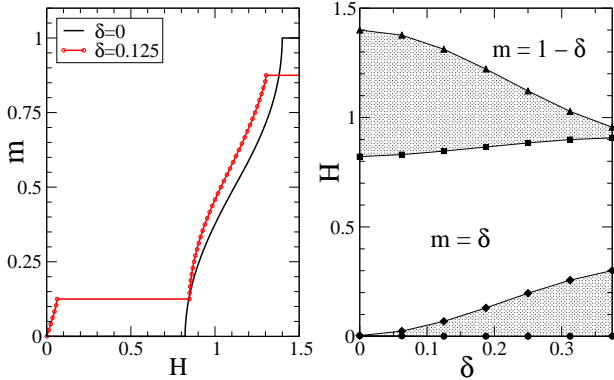


FIG. 5: (Color online) Plateaus phase diagram of a 2-leg ladder for $t_{\perp} = J_{\perp} = 1.0$ and $t_{\parallel} = J_{\parallel} = 0.2$. Doping immediately destroys the $m = 0$ plateau present at half-filling while a large doping-dependent $m = \delta$ plateau appears for a small critical field.

and the partner electron on the rung holds the polarization. The difference between the energies per rung of these two states is:

$$\begin{aligned} m < \delta : \quad \Delta e &\sim (J_{\perp} - 2t_{\perp} - 2t_{\parallel})\delta - J_{\perp}m \\ m > \delta : \quad \Delta e &\sim (2J_{\perp} - 2t_{\perp} - 2t_{\parallel})\delta - 2J_{\perp}m \end{aligned}$$

If $J_{\perp}/(t_{\perp} + t_{\parallel}) > 2$, a transition is then possible from the state with paired holes to the state with unpaired holes. The corresponding critical magnetization $m_c = [1 - 2(t_{\perp} + t_{\parallel})/J_{\perp}]\delta$ is always smaller than δ . This also gives a possible scenario for a wide $m = \delta$ plateau due to interactions. For large J_{\perp} and $m = 0$, we expect the ground state to have pairs of holes and singlets mostly on rungs so that the system has a large spin gap, which gives a $m = 0$ plateau. However, the $m = 0$ plateau is much smaller than the half-filling spin gap because polarized spins in fact gain kinetic energy if they are localized next to holes so that it is easier to create them. As the magnetic field is increased, hole pairs are split as suggested

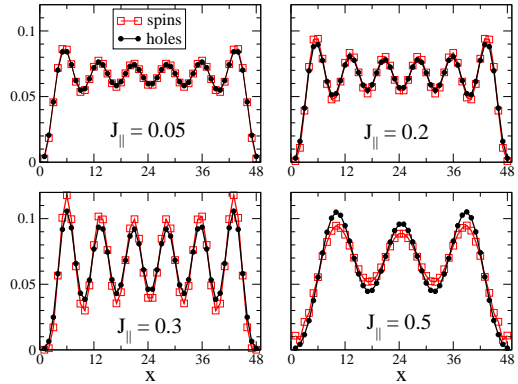


FIG. 6: (Color online) Local densities of holes and spins in a system with $L = 48$ and 6 holes, $t_{\perp} = t_{\parallel} = 1.0$ and $J_{\perp} = 0.5$ (isotropic ladder). As J_{\parallel} is increased, holes pairs form in the $m = \delta$ plateau ground-state. Pairing in and above $m = \delta$ is not expected in the strong-coupling limit.

by the above argument and the partner electron of the hole on the rung becomes polarized. When all of them are fully polarized, we enter the $m = \delta$ plateau because the next spin excitation one can do is to flip a singlet on a rung, which cost is approximately J_{\perp} . The $m = \delta$ plateau can thus be wider than the $m = 0$ one. This scenario corresponds to FIG. 4, where no pairing is found in the plateau from the computation of local densities of spins and holes with DMRG. Such a scenario could be relevant for compounds with lightly coupled dimers which could be doped with holes.

When one starts with unpaired holes at zero magnetic field, for instance with $t_{\parallel} = J_{\parallel} \ll t_{\perp} = J_{\perp}$, the large half-filled spin gap of order $J_{\perp} - J_{\parallel}$ is immediately destroyed by doping (see FIG. 5). Increasing the magnetic field further brings quickly the system into a plateau phase with unpaired holes. While the magnetization curve is similar to the non-interacting one below the $m = \delta$ plateau, its width is clearly controlled by $J_{\perp} - J_{\parallel}$ rather than by $2(t_{\perp} - 2t_{\parallel})$.

An interesting feature on the pairing of holes in the $m = \delta$ plateau is the occurrence of a transition when J_{\parallel} is increased from 0 to J_{\perp} from a state with unpaired holes to paired holes (see FIG. 6). Having pairing in this plateau is a situation that is not expected in the strong-coupling limit as we have seen, but for intermediate J_{\perp} , we expect that hopping between hole pairs and magnons can stabilize hole pairs²¹ (see Sec. IV). FIG. 6 suggests that a J_{\parallel} comparable to J_{\perp} is also needed to have pairing in this phase.

IV. COUPLED BANDS REGIME

A. Bosonized Hamiltonian

When the interactions are not too strong compared to the interchain hopping, it is reasonable to begin to

solve the non-interacting band structure and then add interactions. This is the approach followed in Refs. [30–32]. The non-interacting band structure is simply formed of the bonding band of energy $\varepsilon_{0,\sigma}(k)$ and an antibonding band of energy $\varepsilon_{\pi,\sigma}(k)$. The annihilation operators of the fermions in these bands are respectively given by:

$$\begin{aligned}\psi_{0,\sigma} &= \frac{1}{\sqrt{2}}(\psi_{1,\sigma} + \psi_{2,\sigma}) \\ \psi_{\pi,\sigma} &= \frac{1}{\sqrt{2}}(\psi_{1,\sigma} - \psi_{2,\sigma})\end{aligned}$$

with 1 and 2 the labels of the chains. In the continuum limit, the fermions 0 and π are bosonized in terms of the boson fields $\phi_{k_y,\sigma}$ ($k_y = 0, \pi$) so that we write the fermion operator:

$$\begin{aligned}c_{n,k_y,\sigma} &\rightarrow \sqrt{a} \psi_{k_y,\sigma}(x) \\ &= \sqrt{a}[e^{ik_{F,k_y}^\sigma x} \psi_{R,k_y,\sigma}(x) + e^{-ik_{F,k_y}^\sigma x} \psi_{L,k_y,\sigma}(x)]\end{aligned}\quad (6)$$

in which $x = na$ (a is the lattice spacing) and

$$\psi_{R/L,k_y,\sigma} = \frac{\eta_{R/L,k_y,\sigma}}{\sqrt{2\pi\alpha}} e^{i\epsilon_{R/L}\phi_{R/L,k_y,\sigma}}$$

where R, L are the labels for the right and left movers (see FIG. 7), α is a cutoff (typically a), $\epsilon_{R/L} = \mp 1$ and the η are Klein factors needed to make the annihilation operators of the different fermions species anticommute. We also have the definitions $\phi_{k_y,\sigma} = \frac{1}{2}[\phi_{L,k_y,\sigma} + \phi_{R,k_y,\sigma}]$ while dual fields are $\theta_{k_y,\sigma} = \frac{1}{2}[\phi_{L,k_y,\sigma} - \phi_{R,k_y,\sigma}] = \pi \int \Pi_{k_y,\sigma}$.

We then introduce the useful bosons ϕ_{ν,k_y} with $\nu = c, s$ for charge (resp. spin) corresponding to the symmetric (resp. antisymmetric) combination of $\phi_{k_y,\uparrow}$ and $\phi_{k_y,\downarrow}$. The same transformation is performed on the dual fields, leading to the Hamiltonian:

$$\mathcal{H} = \sum_{\substack{k_y=0,\pi \\ \nu=c,s}} \int \frac{dx}{2\pi} [u_{k_y}(\pi \Pi_{\nu,k_y})^2 + u_{k_y}(\partial_x \phi_{\nu,k_y})^2],$$

where $[\phi_{\nu,k_y}(x), \Pi_{\nu',k'_y}(x')] = i\delta_{\nu,\nu'}\delta_{k_y,k'_y}\delta(x - x')$. In the following, we will make the usual approximation³⁴ of neglecting the difference between the velocities u_{k_y} of the 0 and π bands. This allows us to introduce the linear combinations:

$$\begin{aligned}\phi_{c,\pm} &= \frac{1}{\sqrt{2}}(\phi_{c,0} \pm \phi_{c,\pi}), \\ \phi_{s,\pm} &= \frac{1}{\sqrt{2}}(\phi_{s,0} \pm \phi_{s,\pi}),\end{aligned}$$

with similar definitions for the dual fields $\theta_{\nu,\pm} = \pi \int \Pi_{\nu,\pm}$. In the most general case, we have to use a Z matrix to describe the evolution of the system under magnetic field³⁵. When comparing the results with the chain models of Sec. V, it is useful to note that while $\phi_{c+} = \phi_{\rho+}$ and $\phi_{s+} = \phi_{\sigma+}$ (we use Greek letters for the fields defined in the chain models and Latin letters for

the fields defined in the band models), while there is no simple relation between $\phi_{\rho-}$ and ϕ_{c-} and between ϕ_{s-} and $\phi_{\sigma-}$. The magnetic field couples to the system by a term:

$$\mathcal{H} = \frac{H}{\pi} \int dx \partial_x \phi_{s+} \quad (7)$$

Once interactions are turned on, two types of terms appear in the Hamiltonian. The terms of the first type are forward scattering interaction terms that are quadratic in the fields $\phi_{\nu,\pm}$. The terms of the second type are backscattering interaction terms, the expressions of which were derived in Ref. [31]. Since terms containing $\cos 2\phi_{s+}$ cannot appear in the Hamiltonian when the magnetization is nonzero, the expression of the backscattering terms in a magnetized ladder reads:

$$\mathcal{H}_{\text{back.}} = \int dx \cos 2\theta_{c-} \left[\frac{2g_A}{(2\pi\alpha)^2} \cos 2\phi_{s-} + \frac{2g_B}{(2\pi\alpha)^2} \cos 2\theta_{s-} \right] \quad (8)$$

From the Hamiltonian (8), one sees that in the ground state the field θ_{c-} is pinned to $\langle \theta_{c-} \rangle = 0$. By using the results of Ref. [36] [Sec. 3.1 and Eqs. (20) and (56)], one can argue that in the presence of repulsive interactions, one must have $K_{s-} < 1$. Thus, one obtains a freezing of the field related to the most relevant operator $\langle \phi_{s-} \rangle = \frac{\pi}{2}$. Briefly, when $m = \delta = 0$, all fields are massive and we have the famous spin-liquid phase, often denoted by C0S0. When $m = 0$ but $\delta \neq 0$, the system with repulsive interactions is in a C1S0 phase, or Luther-Emery phase (LE), with sectors $c-$ and $s\pm$ being massive while the sector $c+$ is massless, corresponding to the charge mode. When $m \neq 0$ and $\delta \neq 0$, the sector $s+$ becomes massless giving rise to a C1S1 phase. Luttinger exponents associated with these sectors will be denoted by $K_{c/s+}$. Till now, we have discussed the case of generic nonzero magnetization. For the specific case $m = \delta$, however, a magnetization plateau can be expected. Following Ref. [24], we introduce the fields

$$\phi_\sigma^\pm = \frac{1}{\sqrt{2}}(\phi_{c,\pm} + \sigma \phi_{s,\pm}) \quad (9)$$

which appear in the term that induces the opening of the $m = \delta$ plateaus

$$\int dx \cos [2(k_{F,0}^\sigma + k_{F,\pi}^\sigma)x - 2\sqrt{2}\phi_\sigma^+] \quad (10)$$

with, from (3) and (4), the relation $k_{F,0}^\sigma + k_{F,\pi}^\sigma = \pi(n + \sigma m)$. This term leads to the opening of plateaus when $n \pm m \in \mathbb{Z}$ as expected in YOA theorem. This condition is a commensurability condition which combines both spin and charge degrees of freedom. The $m = \delta$ plateau corresponds to the locking of the ϕ_\uparrow^+ mode. The origin of the term (10) giving rise to the plateau is the Hubbard interaction $U n_{i\uparrow} n_{i\downarrow}$ which contains the terms

$$(c_{0\uparrow}^\dagger c_{\pi\uparrow} + c_{\pi\uparrow}^\dagger c_{0\uparrow})(c_{0\downarrow}^\dagger c_{\pi\downarrow} + c_{\pi\downarrow}^\dagger c_{0\downarrow}), \quad (11)$$

which, once bosonized, yields Umklapp terms such as

$$\int dx \cos [2(k_{F,0}^\uparrow + k_{F,\pi}^\uparrow)x - 2(\phi_{0,\uparrow} + \phi_{\pi,\uparrow})]. \quad (12)$$

B. Superconducting order parameters and most divergent fluctuations

In this section, we define the order parameters for superconductivity at nonzero magnetization (high field), derive their bosonized expressions and deduce their long range correlations. Since the SU(2) symmetry is broken by the magnetic field, we have to compute the superconducting correlation functions $\langle \Delta_{\sigma\sigma'}^\lambda(x) \Delta_{\sigma\sigma'}^{\lambda\dagger}(0) \rangle$ in various channels λ . We use the following microscopic definitions for the pairing operators $\Delta_{\sigma\sigma'}^\lambda(n)$ at rung n :

$$\text{singlet: } \Delta_{\uparrow\downarrow}^s(n) = \sum_{\sigma} \sigma c_{r\sigma} c_{r'-\sigma} \quad (13)$$

$$\text{triplet: } \begin{cases} \Delta_{\uparrow\downarrow}^t(n) = \sum_{\sigma} c_{r\sigma} c_{r'-\sigma} \\ \Delta_{\uparrow\uparrow}^t(n) = c_{r\uparrow} c_{r'\uparrow} \\ \Delta_{\downarrow\downarrow}^t(n) = c_{r\downarrow} c_{r'\downarrow} \end{cases} \quad (14)$$

with $r = (n, 1)$ and $r' = (n, 2)$ for next-nearest neighbor pairs created on a rung and $r = (n, p)$ and $r' = (n+1, p)$ if created on the leg p . Contrarily to the case of the coupled chain regime (Sec. V) where the Fermi wave-vectors are the same in both chains, in the case of the band regime the Fermi wave-vectors of the two bands are different ($k_{F,0}^\sigma \neq k_{F,\pi}^\sigma$) as can be seen on FIG. 1. As a result, a more detailed derivation of the bosonized expressions starting from lattice expressions in a two-chain Hubbard model becomes necessary.

1. Bosonized form

Using the bosonized form (6) of the fermion operators, we can express these order parameters as a function of products of the $\psi_{R/L,k_y,\sigma}$. In this section, only components with the dominant contribution will be kept, i.e. we will neglect terms of the form $\psi_R \psi_R$ and $\psi_L \psi_L$. These dominant contributions correspond to pairing with the lowest total momentum q . The case of $2k_F$ triplet pairing will be discussed in Sec. IV B 2. At finite magnetization, the equality of the velocities and equation (4) ensures that the lowest momentum is $q = k_{F,0/\pi}^\uparrow - k_{F,0/\pi}^\downarrow = \pi m$. To simplify the expression of the operators we will use extensively the following results on a pinned field φ (for which $\langle \varphi \rangle = \text{cste}$): we can replace $\langle f(\varphi) \rangle$ by $f(\langle \varphi \rangle)$ and the dual field has exponentially decaying correlation functions³⁷.

Starting with the interband order parameters, which read:

$$\begin{aligned} \psi_{R,0,\sigma} \psi_{L,\pi,-\sigma} &\sim e^{i[\theta_{c+} - \phi_{c-} - \sigma(\phi_{s+} - \phi_{s-})]}, \\ \psi_{R,0,\sigma} \psi_{L,\pi,\sigma} &\sim e^{i[\theta_{c+} - \phi_{c-} - \sigma(\theta_{s+} - \phi_{s-})]}, \end{aligned}$$

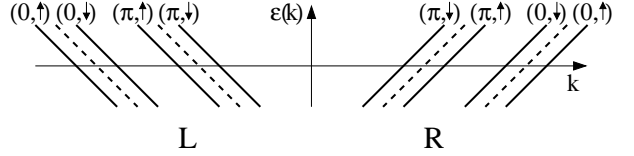


FIG. 7: Schematic representation of bosonized bands in the coupled band models.

we note that they are all proportional to $e^{i\phi_{c-}}$ and thus, since θ_{c-} is pinned, their correlations decay exponentially. In other words, power law decay is possible only for intraband superconducting correlations.

The intraband superconducting order parameters in the three spin channels read respectively:

-Intraband singlet:

$$\begin{aligned} \sum_{\sigma} \sigma \psi_{R,0,\sigma} \psi_{L,0,-\sigma} &\sim \sum_{\sigma} \sigma e^{i[\theta_{c+} + \theta_{c-} - \sigma(\phi_{s+} + \phi_{s-})]}, \\ \sum_{\sigma} \sigma \psi_{R,\pi,\sigma} \psi_{L,\pi,-\sigma} &\sim \sum_{\sigma} \sigma e^{i[\theta_{c+} - \theta_{c-} - \sigma(\phi_{s+} - \phi_{s-})]}. \end{aligned}$$

-Intraband triplet $S^z = 0$:

$$\begin{aligned} \sum_{\sigma} \psi_{R,0,\sigma} \psi_{L,0,-\sigma} &\sim \sum_{\sigma} e^{i[\theta_{c+} + \theta_{c-} - \sigma(\phi_{s+} + \phi_{s-})]}, \\ \sum_{\sigma} \psi_{R,\pi,\sigma} \psi_{L,\pi,-\sigma} &\sim \sum_{\sigma} e^{i[\theta_{c+} - \theta_{c-} - \sigma(\phi_{s+} - \phi_{s-})]}. \end{aligned}$$

-Intraband triplet $S^z = 1$:

$$\begin{aligned} \psi_{R,0,\sigma} \psi_{L,0,\sigma} &\sim e^{i[\theta_{c+} + \theta_{c-} + \sigma(\theta_{s+} + \theta_{s-})]}, \\ \psi_{R,\pi,\sigma} \psi_{L,\pi,\sigma} &\sim e^{i[\theta_{c+} - \theta_{c-} + \sigma(\theta_{s+} - \theta_{s-})]}. \end{aligned}$$

To determine which forms of superconductivity will be dominant, we need to express the leg and rung order parameters in terms of the intraband order parameters. We have for the rung singlet order parameter,

$$\Delta_{\uparrow\downarrow}^s(x) \sim \sum_{\sigma} \frac{\sigma}{2} e^{i\sigma qx} (\psi_{R,0,\sigma} \psi_{L,0,-\sigma} - \psi_{R,\pi,\sigma} \psi_{L,\pi,-\sigma}), \quad (15)$$

Whereas the rung triplet $S^z = 0$ is given by:

$$\Delta_{\uparrow\downarrow}^t(x) \sim \sum_{\sigma} \frac{1}{2} e^{i\sigma qx} (\psi_{R,\pi,\sigma} \psi_{L,0,-\sigma} - \psi_{R,0,-\sigma} \psi_{L,\pi,\sigma}), \quad (16)$$

therefore, since it is composed only of interband terms, we expect that its correlation will present exponential decay. Lastly, for the rung triplet $S^z = 1$ order parameter, we find:

$$\Delta_{\uparrow\uparrow}^t(x) \sim \frac{1}{2} (\psi_{R,0,\uparrow} \psi_{L,0,\uparrow} - \psi_{R,\pi,\uparrow} \psi_{L,\pi,\uparrow}), \quad (17)$$

Turning to the leg singlet order parameter, we find that it reads:

$$\Delta_{\uparrow\downarrow}^s(x) \sim \sum_{\sigma} \frac{\sigma}{2} e^{i\sigma qx} \left[e^{-ik_{F,0}^{-\sigma} a} \psi_{R,0,\sigma} \psi_{L,0,-\sigma} + (0 \rightarrow \pi) \right]. \quad (18)$$

Note that because we can neglect interband coupling, the expression is the same on both legs. Thus leg-leg correlations on the same leg and between the legs will have the same sign as found numerically in FIG. 8. Analogously, the leg triplet $S^z = 0$ operator reads:

$$\Delta_{\uparrow\downarrow}^t(x) \sim \sum_{\sigma} \frac{1}{2} e^{i\sigma qx} [\sin(k_{F,0}^{\sigma} a) \psi_{R,0,\sigma} \psi_{L,0,-\sigma} + (0 \rightarrow \pi)]. \quad (19)$$

Note that if we take the limit $a \rightarrow 0$ this term disappears as happened for the rung triplet. Finally, the leg triplet $S^z = 1$ reads:

$$\Delta_{\uparrow\uparrow}^t(x) \sim \frac{1}{2} [e^{-ik_{F,0}^{\sigma} a} \psi_{R,0,\uparrow} \psi_{L,0,\uparrow} + (0 \rightarrow \pi)]. \quad (20)$$

Since $K_{s-} < 1$, we have $\langle \phi_{s-} \rangle = \frac{\pi}{2}$. Then, all the intraband triplet $S^z = 1$ have exponentially decaying correlations. As a consequence, both the leg and the rung triplets with $S^z = 1$ have exponentially decaying correlations. The behavior of these correlations with higher $2k_F$ momentum will be discussed in Sec. IV B 2. Another consequence of the ordering of the field ϕ_{s-} is that:

$$\begin{aligned} \psi_{R,0,\sigma} \psi_{L,0,-\sigma} &\sim e^{-i\frac{\pi}{2}\sigma} e^{i(\theta_{c+} - \sigma\phi_{s+})}, \\ \psi_{R,\pi,\sigma} \psi_{L,\pi,-\sigma} &\sim e^{i\frac{\pi}{2}\sigma} e^{i(\theta_{c+} - \sigma\phi_{s+})}. \end{aligned}$$

Provided that $k_{F,0} \neq k_{F,\pi}$, the leg triplet $S^z = 0$ order parameter does not vanish. We find that it has the same critical exponent as the rung singlet order parameter, namely $\frac{1}{2}(K_{c+}^{-1} + K_{s+})$. It is larger than the $m = 0$ critical exponent $1/(2K_{c+})$ because of the appearance of the massless boson θ_{s+} . The fact that we have a finite momentum pairing with $q = \pi m$ which is very likely to occur in a one-dimensional-like system and is the signature of the FFLO mechanism.

2. $S^z = 1$ Triplet with a $2k_F$ momentum

Another notable result is the presence of rung-rung triplet $S^z = 1$ correlations with $2k_F$ oscillations. Within the band representation, it is indeed possible to find a component of the rung-rung triplet correlations that has power law decay. Let us consider the next terms in the expansion of the rung triplet operator:

$$\psi_{1,\sigma} \psi_{2,\sigma} \sim -2e^{i(k_{F,0}^{\sigma} + k_{F,\pi}^{\sigma})x} \psi_{R,0,\sigma} \psi_{R,\pi,\sigma} + \dots$$

In bosonized form, this operator reads:

$$\Delta_{\sigma\sigma,2k_F}^t(x) \sim e^{i(k_{F,0}^{\sigma} + k_{F,\pi}^{\sigma})x} e^{i[\theta_{c+} - \phi_{c+} + \sigma(\theta_{s+} - \phi_{s+})]}$$

It has power law correlations with a critical exponent

$$\frac{1}{2} (K_{c+} + K_{c+}^{-1} + K_{s+} + K_{s+}^{-1}),$$

and, from equations (3) and (4), the associated wave-vector is $k_{F,0}^{\sigma} + k_{F,\pi}^{\sigma} = \pi(n + \sigma m)$. Note that its critical exponent is always larger than the one of the rung singlet order parameter.

3. Charge-density waves order parameters

Here, we address the question of the CDW exponents under magnetic field. First, the $2k_F$ CDW order parameter n_i , which vanishes exponentially at zero magnetization, contains terms such as:

$$\psi_{r,0\sigma}^{\dagger} \psi_{r,\pi\sigma} \sim e^{i[\phi_{c-} + \sigma\phi_{s-} - r(\theta_{c-} + \sigma\theta_{s-})]}$$

with $r = \pm$ for R, L and a wave-vector $k_{F,\pi}^{\sigma} - k_{F,0}^{\sigma}$. These order parameters decay exponentially because they are proportional to $e^{i\phi_{c-}}$. A last possible term is

$$\psi_{R,0\sigma}^{\dagger} \psi_{L,\pi\sigma} \sim e^{i[\phi_{c+} - \theta_{c-} + \sigma(\phi_{s+} - \theta_{s-})]}$$

with a “ $2k_F$ ” wave vector $\pi(n + \sigma m)$. It decays exponentially because of $e^{i\theta_{s-}}$. Finally, no $2k_F$ CDW are expected under magnetic field.

Secondly, the $4k_F$ CDW order parameter¹⁴ is n_i^2 and has an exponent $2K_{c+}$ at zero magnetization. This order parameter contains terms such as

$$\psi_{R,0\sigma}^{\dagger} \psi_{L,0\sigma} \psi_{R,\pi\sigma}^{\dagger} \psi_{L,\pi\sigma} \sim e^{i2[\phi_{c+} + \sigma\phi_{s+}]}$$

which have a “ $4k_F$ ” wave vector $2\pi(n + m)$ and, for nonzero magnetization, an exponent $2(K_{c+} + K_{s+})$. We also have terms like

$$\psi_{R,0\sigma}^{\dagger} \psi_{L,0\sigma} \psi_{R,\pi-\sigma}^{\dagger} \psi_{L,\pi-\sigma} \sim e^{i2[\phi_{c+} + \sigma\phi_{s-}]}$$

with a wave-vector $2(k_{F,0}^{\sigma} + k_{F,\pi}^{-\sigma})$ and an exponent $2K_{c+}$ which is not affected by the magnetic field. This last term can compete with the superconducting order parameter to be the most diverging fluctuations depending on K_{c+} and K_{s+} .

C. Interpreting the superconducting critical field H_c as a band-filling transition

In this section, we identify the observed superconducting upper critical field H_c with a band-filling transition. Such a transition will ungap all 3 remaining sectors, leading to an enhancement of the correlations exponents. We describe the system just above the transition and compute the various possible exponents using bosonization. We consider a case where the Fermi energy is positioned in such a way that the band (π, \downarrow) is empty while the three other bands remain partially filled (see FIG. 1 for illustration). The band (π, \downarrow) being empty has important consequences. Projecting out the high energy subspace where the band $(0, \downarrow)$ is occupied by a single electron, one gets in lowest order:

$$c_{n,p,\downarrow}^{\dagger} c_{n,p,\downarrow} \rightarrow \frac{1}{2} c_{n,0,\downarrow}^{\dagger} c_{n,0,\downarrow}, \quad (21)$$

and as a result the on-site Hubbard interaction reduces to:

$$\frac{U}{2} \sum_n n_{i,0,\downarrow} (n_{i,0,\uparrow} + n_{i,\pi,\uparrow}). \quad (22)$$

Type of operator	fermion expression	dimension	wave-vector
$S^z = 1$ triplet	$\psi_{R0\uparrow}\psi_{L0\uparrow}$	$\frac{1}{4K_1} + \frac{1}{4K_2} + \frac{1}{2K_3}$	0
	$\psi_{R\pi\uparrow}\psi_{L\pi\uparrow}$	$\frac{1}{4K_1} + \frac{1}{4K_2} + \frac{1}{2K_3}$	0
	$\psi_{R0\downarrow}\psi_{L0\downarrow}$	$\frac{1}{2K_1} + \frac{1}{2K_2}$	0
	$\psi_{R\pi\downarrow}\psi_{L0\downarrow}$	$\frac{1}{4K_1} + \frac{1}{4K_2} + \frac{K_3}{2}$	$k_{F\pi}^\uparrow - k_{F0}^\uparrow$
$S^z = 0$ triplet or singlet	$\psi_{R0\uparrow}\psi_{L0\downarrow}$	$\frac{3+\sqrt{8}}{16}(K_1^{-1} + K_2) + \frac{3-\sqrt{8}}{16}(K_2^{-1} + K_1) + \frac{1}{8}(K_3 + K_3^{-1})$	$k_{F0}^\uparrow - k_{F0}^\downarrow$
	$\psi_{R\pi\uparrow}\psi_{L0\downarrow}$	$\frac{3+\sqrt{8}}{16}(K_1^{-1} + K_2) + \frac{3-\sqrt{8}}{16}(K_2^{-1} + K_1) + \frac{1}{8}(K_3 + K_3^{-1})$	$k_{F\pi}^\uparrow - k_{F0}^\downarrow$

TABLE I: The superconducting operators for the Hubbard model with an empty band corresponding to the coupled band regime just above H_c .

Type of operator	fermion expression	dimension	wave-vector
SDW^z/CDW	$\psi_{R0\uparrow}^\dagger\psi_{L0\uparrow}$	$\frac{K_1}{4} + \frac{K_2}{4} + \frac{K_3}{2}$	$2k_{F0}^\uparrow$
	$\psi_{R\pi\uparrow}^\dagger\psi_{L\pi\uparrow}$	$\frac{K_1}{4} + \frac{K_2}{4} + \frac{K_3}{2}$	$2k_{F\pi}^\uparrow$
	$\psi_{R0\downarrow}^\dagger\psi_{L0\downarrow}$	$\frac{K_1}{2} + \frac{K_2}{2}$	$2k_{F0}^\downarrow$
	$\psi_{R\pi\downarrow}^\dagger\psi_{L0\downarrow}$	$\frac{K_1}{4} + \frac{K_2}{4} + \frac{1}{2K_3}$	$k_{F\pi}^\uparrow + k_{F0}^\uparrow$
$SDW^{x,y}$	$\psi_{R0\uparrow}^\dagger\psi_{L0\downarrow}$	$\frac{3-\sqrt{8}}{16}(K_1^{-1} + K_2) + \frac{3+\sqrt{8}}{16}(K_2^{-1} + K_1) + \frac{1}{8}(K_3 + K_3^{-1})$	$k_{F0}^\uparrow + k_{F0}^\downarrow$
	$\psi_{R\pi\uparrow}^\dagger\psi_{L0\downarrow}$	$\frac{3-\sqrt{8}}{16}(K_1^{-1} + K_2) + \frac{3+\sqrt{8}}{16}(K_2^{-1} + K_1) + \frac{1}{8}(K_3 + K_3^{-1})$	$k_{F\pi}^\uparrow + k_{F0}^\downarrow$

TABLE II: The CDW/SDW operators for the Hubbard model with an empty band corresponding to the coupled band regime just above H_c .

In the absence of commensuration between the different bands, the resulting bosonized Hamiltonian has only forward scattering interactions. Thus, its excitations are completely gapless. The bosonized Hamiltonian reads:

$$\mathcal{H} = \mathcal{H}_0 + \mathcal{H}_U \quad (23)$$

$$\mathcal{H}_0 = \sum_{\nu \in \{(0,\uparrow), (0,\downarrow), (\pi,\uparrow)\}} \int \frac{dx}{2\pi} v_{F,\nu} [(\pi\Pi_\nu)^2 + (\partial_x\phi_\nu)^2]$$

$$\mathcal{H}_U = \frac{U\alpha}{2\pi^2} \int dx \partial_x\phi_{0,\downarrow} (\partial_x\phi_{0,\uparrow} + \partial_x\phi_{\pi,\uparrow}) \quad (24)$$

This Hamiltonian can be fully diagonalized. In the general case, where the Fermi velocities are all different, one needs first to perform a rescaling: $\Pi_\nu \rightarrow \sqrt{u/v_{F,\nu}}\Pi_\nu$ and $\phi_\nu \rightarrow \phi_\nu/\sqrt{u/v_{F,\nu}}$ where u is an arbitrary quantity with the dimension of a velocity and then diagonalize the matrix:

$$\begin{pmatrix} v_{F,0\uparrow}^2 & \frac{U\alpha}{4\pi^2}\sqrt{v_{F,0\uparrow}v_{F,0\downarrow}} & 0 \\ \frac{U\alpha}{4\pi^2}\sqrt{v_{F,0\uparrow}v_{F,0\downarrow}} & v_{F,0\downarrow}^2 & \frac{U\alpha}{4\pi^2}\sqrt{v_{F,\pi\uparrow}v_{F,0\downarrow}} \\ 0 & \frac{U\alpha}{4\pi^2}\sqrt{v_{F,0\uparrow}v_{F,0\downarrow}} & v_{F,\pi\uparrow}^2 \end{pmatrix} \quad (25)$$

Afterwards, one performs the inverse rescaling on the diagonal matrix to obtain the velocities of the modes and the associated Luttinger exponents. To simplify the algebra, we will assume that all the Fermi velocities are equal. Then, we find that the following combination of fields

$$\begin{pmatrix} \phi_1 \\ \phi_2 \\ \phi_3 \end{pmatrix} = \begin{pmatrix} \frac{\sqrt{2}}{2} & \frac{1}{2} & \frac{1}{2} \\ \frac{\sqrt{2}}{2} & -\frac{1}{2} & -\frac{1}{2} \\ 0 & \frac{\sqrt{2}}{2} & -\frac{\sqrt{2}}{2} \end{pmatrix} \begin{pmatrix} \phi_{0,\downarrow} \\ \phi_{0\uparrow} \\ \phi_{\pi\uparrow} \end{pmatrix}, \quad (26)$$

diagonalizes the interaction. and:

$$u_1 K_1 = u_2 K_2 = u_3 K_3 = v_F \quad (27)$$

$$\frac{u_1}{K_1} = v_F + \frac{U\alpha}{2\pi^2\sqrt{2}} \quad (28)$$

$$\frac{u_2}{K_2} = v_F - \frac{U\alpha}{2\pi^2\sqrt{2}} \quad (29)$$

$$\frac{u_3}{K_3} = v_F \quad (30)$$

In terms of these new fields, the fermion operators read:

$$\psi_{r,0,\uparrow} = \frac{\eta_{r,0,\uparrow}}{\sqrt{2\pi\alpha}} e^{i[\frac{1}{2}(\theta_1-r\phi_1)-\frac{1}{2}(\theta_2-r\phi_2)+\frac{1}{\sqrt{2}}(\theta_3-r\phi_3)]}$$

$$\psi_{r,\pi,\uparrow} = \frac{\eta_{r,\pi,\uparrow}}{\sqrt{2\pi\alpha}} e^{i[\frac{1}{2}(\theta_1-r\phi_1)-\frac{1}{2}(\theta_2-r\phi_2)-\frac{1}{\sqrt{2}}(\theta_3-r\phi_3)]}$$

$$\psi_{r,0,\downarrow} = \frac{\eta_{r,0,\downarrow}}{\sqrt{2\pi\alpha}} e^{i\frac{\sqrt{2}}{2}[(\theta_1-r\phi_1)+(\theta_2-r\phi_2)]}$$

From these expressions, it is possible to obtain the various superconducting order parameters and their critical exponents. The results are gathered in table I and table II on which one must note that the correlation exponent will be twice the dimension of the operator.

D. Numerical results on superconducting correlation functions

We have computed superconducting correlation functions with DMRG using the definitions of Eqs. (13) and (14). As predicted by bosonization results, only modified d -wave singlet superconductivity is found when $m = 0$

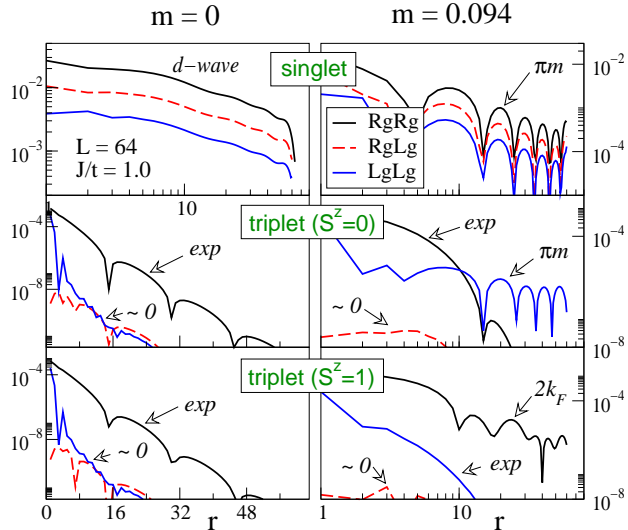


FIG. 8: (Color online) Absolute value of superconducting correlations for zero and a finite magnetization in an isotropic doped ladder with $\delta = 0.063$. Notation are “Rg” for rung, “Lg” for leg, “ ~ 0 ” for numerically irrelevant signal, “exp” for exponentially decaying correlations and “ πm ” and “ $2k_F$ ” for the wave-vectors. Note that the $S^z = 1$ “ $2k_F$ ” oscillations are smoothed out by taking the absolute value. $M = 1000$ states were kept with discarded weight of order 10^{-6} .

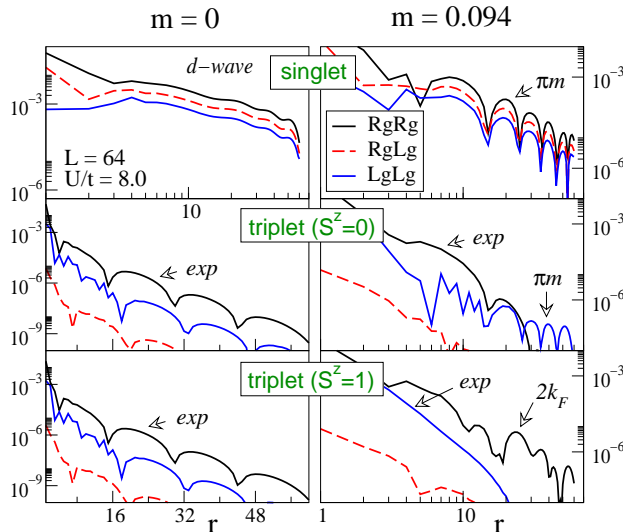


FIG. 9: (Color online) Same correlations as FIG. 8 but using the Hubbard model with $\delta = 0.063$ and $U/t = 8.0$. $M = 1600$ states were kept with discarded weight of order 10^{-6} .

(rung-leg correlations have an opposite sign to rung-rung and leg-leg correlations, see Ref. [14] for a bosonization discussion), while $S^z = 0$ leg-leg triplet and $S^z = 1$ rung-rung triplet correlations emerge under high magnetic field (see FIG. 8 for the t-J model and FIG. 9 for the repulsive Hubbard model). Furthermore, these correlations oscillate with wave-vectors $q = \pi m$ for the $S^z = 0$ channel and $q = 2k_F$ for the $S^z = 1$ channel. The $q = \pi m$ relation has been checked in all the FFLO phase (see

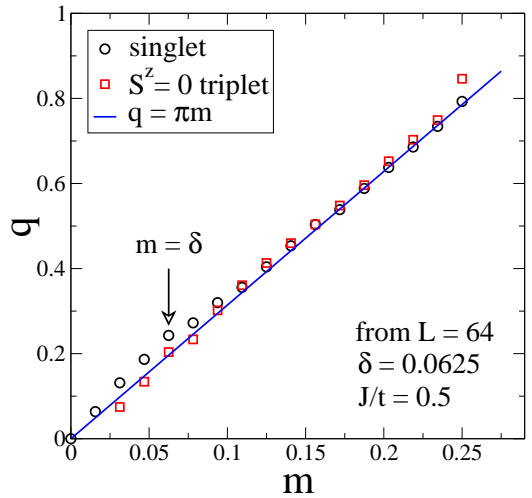


FIG. 10: (Color online) Verification of the $q = \pi m$ relation of FFLO-like pairing at finite magnetization in an isotropic ladder with $J/t = 0.5$.

FIG. 17 and discussion in Sec. IV E), by fitting the oscillating correlations with $A \cos(qr + \varphi)/r^\alpha$ (see FIG.10), confirming the FFLO-like mechanism. We observe that $S^z = 0$ rung-rung triplet correlations have an exponential behavior while rung-rung singlet are algebraic, in agreement with the prediction from bosonization. Since from the point of view of the rotation symmetry these two order parameter transform in the same way, the difference must be caused by their different transformation properties under interchange of the legs. Note that because of the $\sin(k_{F,k_y}^\sigma a)$ factors in the leg singlet and $S^z = 0$ leg triplet, the cancellation of the intraband terms obtained in the case of rung order parameters is absent. This explains the observation of power-law correlations. Concerning the orbital part of pairs, singlet Cooper pairs have a mixed s -wave and d -wave structure and $S^z = 0$ triplet can be considered to first approximation as p -wave pairs along the legs (with a symmetric superposition of the two legs).

The good agreement with bosonization predictions relies on the fact that in the doped isotropic t-J ladder, 4 Fermi points exist with approximatively³³ $k_{F,0} \sim 3\pi/5$ and $k_{F,\pi} \sim 2\pi/5$ when $m = 0$ and that the assumption of equal Fermi velocities is numerically reasonable at low hole doping. The existence of a small leg-leg triplet component (about 100 times smaller than the rung rung triplet) in the two leg t-J ladder considered may therefore be explained by the persistence of a small band splitting in this strongly coupled ladder system.

We now would like to compare precisely the algebraic decay exponents α^s and α^t of the singlet and $S^z = 0$ leg-leg triplet correlations. DMRG is known to often underestimate correlation functions²³ for a fixed number of state kept M . In order to capture the behavior in the thermodynamic limit, we computed the correlation functions for fixed M ranging from 800 to 2000 and lengths

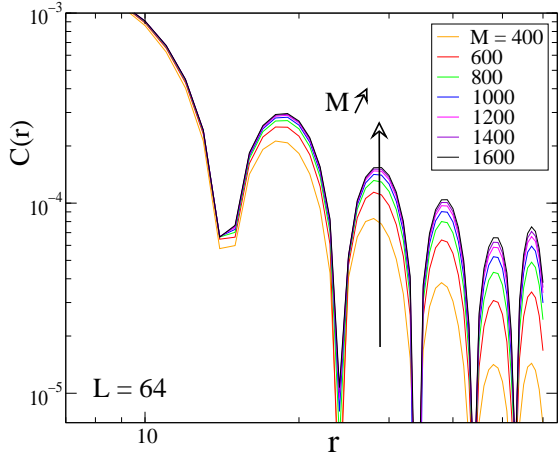


FIG. 11: (Color online) Convergence with the number of kept states M for a fixed length $L = 64$. The plotted superconducting correlation is the singlet one and parameters are $m = 0.094$, $\delta = 0.063$ and $J/t = 0.5$ which corresponds to the phase above the $m = \delta$ plateau and below the superconducting upper critical field H_c .

$L = 32, 64, 96$ and 128 (we worked at fixed $\delta = 1/16$ and $m = 3/32$ so that these are the only accessible cluster sizes). We extracted $\alpha(M, L)$ by fitting the data. Then, we can extrapolate α in the $M \rightarrow \infty$ limit to get a correct exponent $\alpha(L)$ at size L from which we can do a finite size scaling. On FIG. 11, we see that for a given size, $\alpha(M)$ decreases as M is enlarged, roughly like $\alpha(M) \sim 1/M$ (see FIG. 13 (b)) as was previously found. We note from FIG. 12 that the larger the system, the larger M is needed to reach a good convergence. Convergence as a function of the discarded weight is also given on FIG. 13 and has qualitatively the same behavior. For $L = 128$, the convergence is slower with M than for $L = 96$, probably because we would need larger M to have a correct accuracy (the $1/M$ might be realized for large enough M) so that we believe the results are not as reliable as for $L = 64$ and 96 (larger M would be very expensive numerically). On one side of FIG.13 (c), $M = 2000$ is too small (for $L = 128$) while on the other side, it is difficult to extract α because the system is too small to resolve enough oscillations (when $L = 32$). Extrapolations can be tentatively done with some uncertainties which can be roughly estimated. Therefore, we can infer from FIG.13 that $\alpha^s = 1.54 \pm 0.15$ is greater than $\alpha^t = 1.17 \pm 0.15$ which pleads in favor of dominating $S^z = 0$ triplet correlations in this part of the phase diagram (above the $m = \delta$ plateau and below H_c) but the difference is rather small. Finite size effects could explain that the bosonization prediction $\alpha^t = \alpha^s$ is not realized on numerical results. Note that $\alpha < 2$ is sufficient to have a divergent superconducting susceptibility in the system. Concerning CDW exponents, they are difficult to compute numerically because of OBC but we will see that we can deduce from the two-particle gap of FIG. 18 that the system is in a superconducting phase.

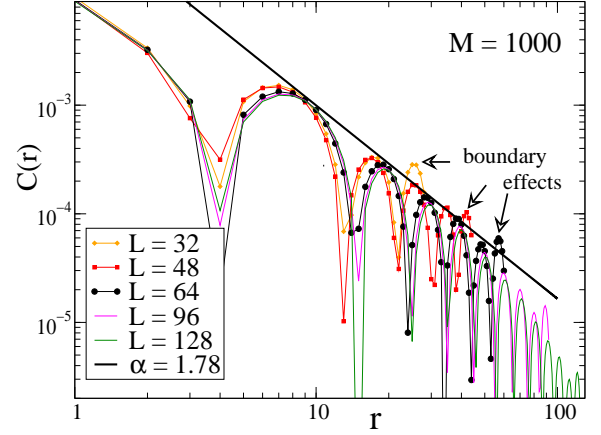


FIG. 12: (Color online) Convergence with size L for the same parameters as in FIG. 11, M being fixed.

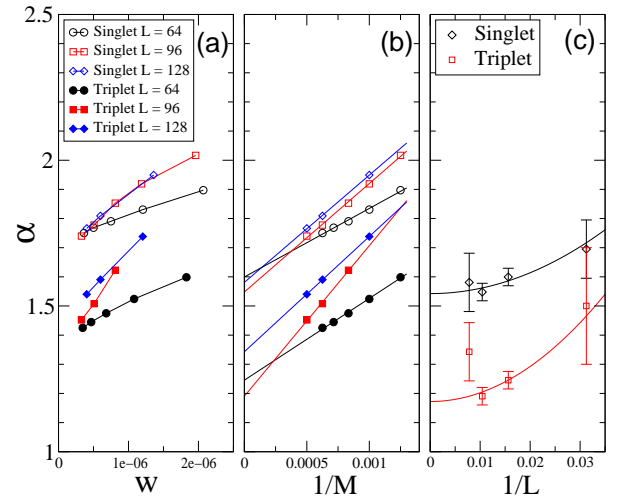


FIG. 13: (Color online) Extrapolation of fitted exponent as a function of discarded weight w (a) and of the inverse of the number of kept states M (b) for different lengths L . Extrapolated results from (b) are tentatively extrapolated vs L in (c). Large error bars occur when L is too small (for $L = 32$) and because M is too small (for $L = 128$). Parameters are given in the caption of FIG.11.

Evolution of the Luttinger parameter K_{s+}

We now want to have access to the evolution of the Luttinger exponent K_{s+} of the gapless mode which appears at finite magnetization. We remark that the bosonized form of the triplet creation operator on a rung $S_2^+(x)S_1^+(x)$ contains dominant terms such as

$$\psi_{L,0\uparrow}^\dagger \psi_{L,0\downarrow} \psi_{R,\pi\uparrow}^\dagger \psi_{R,\pi\downarrow} \sim e^{-i2[\phi_{s-} + \theta_{s+}]}. \quad (31)$$

giving an exponent $2K_{s+}^{-1}$ since $\langle \phi_{s-} \rangle = \pi/2$. The wave-vector associated with this operator is $(k_{F,0}^\uparrow - k_{F,0}^\downarrow) - (k_{F,\pi}^\uparrow - k_{F,\pi}^\downarrow) \sim 0$ since, if the difference between the Fermi velocities of the 0 and π bands is negligible, we have $k_{F,k_y}^\uparrow - k_{F,k_y}^\downarrow = \pi m$. Note that $2K_{s+}^{-1}$ is the smaller ex-

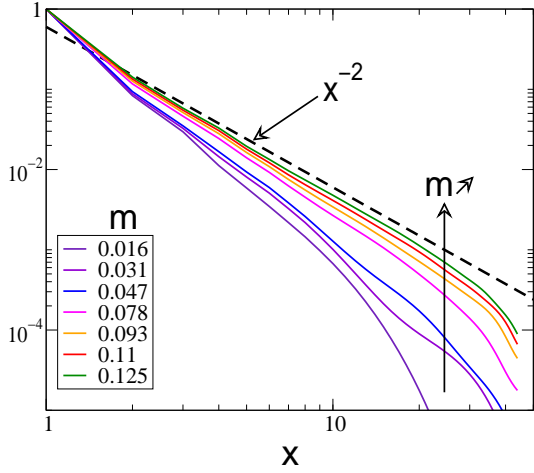


FIG. 14: (Color online) Normalized spin correlations $\langle S_2^+(x)S_1^+(x)S_2^-(0)S_1^-(0) \rangle$ for various magnetization in the isotropic t-J model with $J/t = 0.75$ and $\delta = 0.063$. Their decay exponent is $2K_{s+}^{-1}$ which gives access to $K_{s+}(H)$. Correlations were computed on a system with $L = 64$ and $M = 1200$ states kept.

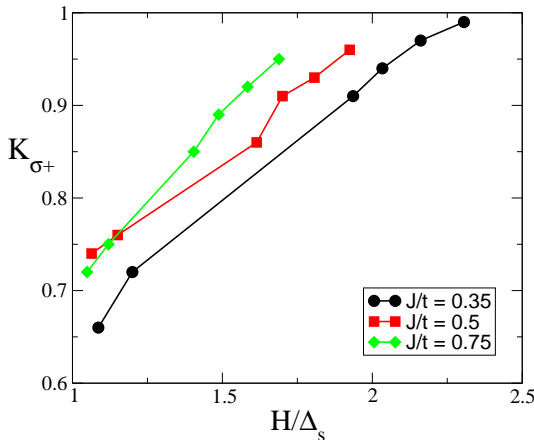


FIG. 15: (Color online) $K_{s+}(H/\Delta_s)$ from DMRG computations on a system with parameters of FIG. 14.

ponent for terms with this wave-vector. Because $K_{s+} < 1$, we could expect smaller possible exponents such as $2K_{s+}$ or $\frac{1}{2}[K_{s+} + K_{s+}^{-1}]$. For the first, one can show that fields $2[\phi_{s+} \pm \phi_{s-}]$ or $2[\phi_{s+} + \sigma\theta_{c-}]$ cannot appear in the decomposition of $S_2^+ S_1^+$. For the other, fields $\phi_{s+} \pm \theta_{s+} \pm \theta_{c-} \pm \phi_{s-}$ cannot be decomposed in terms of the right and left movers fields with factors \pm . Finally, the decay exponent of the correlations of this order parameter is expected to be $2K_{s+}^{-1}$ and depends only on K_{s+} and not on K_{c+} . Numerically, we have computed the correlation function $\langle S_2^+(x)S_1^+(x)S_2^-(0)S_1^-(0) \rangle$. Data for the isotropic t-J model are displayed on FIG. 14 and show a power-law decay with an exponent larger than 2 and a wave-vector approaching zero. Points are given as a function of H/Δ_s , Δ_s being the finite-size spin gap of the system. We thus have access to the evolution of K_{s+}

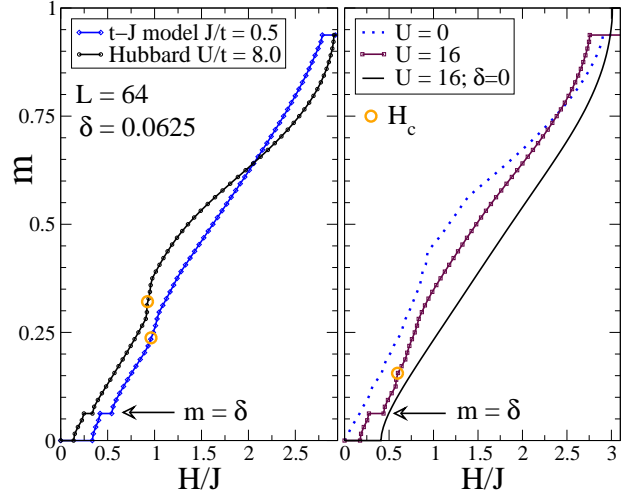


FIG. 16: (Color online) Magnetization curves for the isotropic t-J, Hubbard and non-interacting systems. Irrational plateaus are clearly visible at $m = \delta$. H_c represents the superconducting critical field. The energy scale J is defined as $4t^2/U$ in the Hubbard model. The non-interacting system curve has been rescaled ($H \rightarrow H/4$) for clarity.

as a function of the magnetic field (see FIG. 15). The general behavior is that $K_{s+} < 1$ (as expected) and increases with magnetic field towards the limit $K_{s+} = 1$ at high fields. Lastly, the obtained values for K_{s+} should be slightly larger in the thermodynamic limit than what is found because of finite size and finite M effects as explained above.

E. Generic phase diagram of the t-J model

In this section, we discuss the generic phase diagram in the (H, δ) plane for the isotropic t-J model on the basis of DMRG and bosonization results.

1. Doping-dependent magnetization plateaus

The magnetization curves $m(H)$ of FIG. 16, obtained within the Hubbard and t-J models, display plateaus for $m = 0$ and $m = \delta$. Energies $E(n_h, S^z)$ were computed keeping $M = 1600$ states with the single-site method proposed by White³⁸ (we used a noise level of 10^{-6}) at fixed hole number n_h and total magnetization S^z . Magnetic fields are deduced using $H(S^z) = E(n_h, S^z + 1) - E(n_h, S^z)$, and interpolated with $[H(S^z) + H(S^z - 1)]/2$ if they do not belong to a plateau. The $m = 0$ plateau simply corresponds to the well-known spin-gap of the doped ladder. The $m = \delta$ plateau, exists at small doping for continuous values of δ (see FIG. 17 and Ref. [21]) and thus falls into the classes of doping-dependent irrational magnetization plateaus predicted^{10,24} by Cabra *et al.*. It can be understood as a Commensurate-Incommensurate³⁹ (C-IC) transition so that we expect the critical exponent

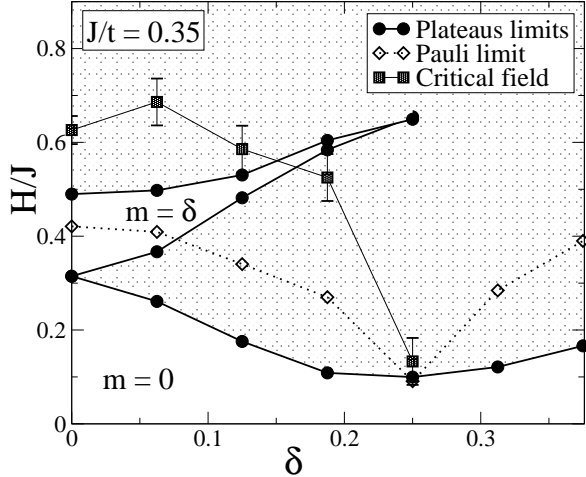


FIG. 17: Phase diagram for the isotropic two-leg t-J ladder in the (H, δ) plane for $J/t = 0.35$. The large FFLO phase is delimited by the upper limit of the $m = 0$ plateau and the critical field H_c . Note also that in this part of the diagram, the $m = \delta$ phase is not expected to be a superconducting phase but rather metallic.

of the magnetization as a function of the magnetic field to be $1/2$. In the plateau phase, the mode ϕ_{\uparrow}^+ is locked but the sector $(\downarrow, +)$ remains gapless, leading to a metallic phase. Note that ϕ_{\uparrow}^+ is a superposition of both spin and charge modes so that charge and spin are no more independent modes in the plateau phase.

The Hubbard and t-J models give qualitatively the same behavior at low magnetization. The spin gap ($m = 0$ plateau) in the Hubbard model with $U/t = 8$ is about half of the spin gap of the t-J model with $J/t = 0.5$ as it was previously found⁴⁰, but the irrational plateau has roughly the same width. A larger U gives a slightly larger plateau. Both models displays a singularity of the magnetization curve, more or less pronounced, near the superconducting critical field H_c . The location of H_c in FIG. 16 have been roughly determined by looking at local densities (see Ref. [21] for method) since Cooper pairs break down above this field. For larger U , the superconducting critical field is smaller. These results are also observed in the t-J model having in mind that $J/t \sim t/U$ (see Sec. IV E 2 and FIG. 19). For higher magnetization states, Gutzwiller projection induces a rather different behavior between strongly interacting systems (Hubbard $U = 16$ and t-J) the Hubbard model with $U = 8$ which displays the expected square-root-like behaviors near critical fields in good agreement with the band-emptying scenario proposed in Sec. IV C. At last, a quick comparison with the isotropic non-interacting system proves the non-trivial role of interactions in the apparition of these plateaus.

The magnetic part of the phase diagram of the t-J model with $J/t = 0.35$ has been computed (see FIG. 17) and is very similar to the one obtained with $J/t = 0.5$ (see Ref. [21]) but have larger $m = \delta$ plateaus. We pro-

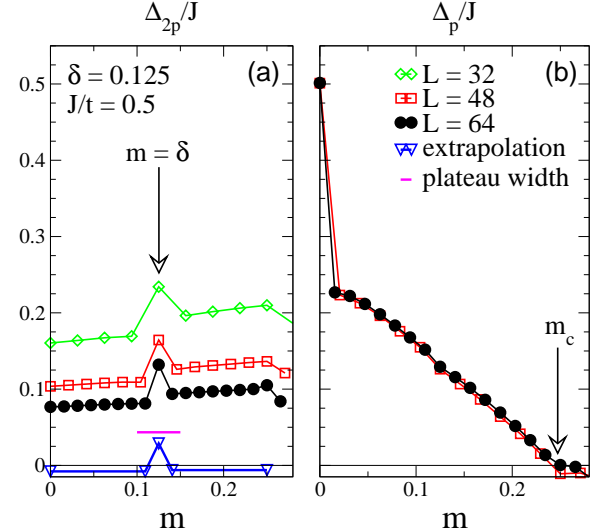


FIG. 18: (Color online) Two-particle gap (a) and pairing energy (b) for isotropic ladders as a function of magnetization. An anomaly in the two-particle gap at $m = \delta$ is clearly visible while the pairing energy remains finite up to the superconducting-metallic state transition. m_c represents the magnetization corresponding to the superconducting critical field H_c .

pose that such a phase diagram is generic for the isotropic t-J and Hubbard models under Zeeman effect at low doping and for parameters $0.25 \lesssim (J/t \sim 4t/U) \lesssim 1.0$ corresponding to the strong-coupling regime. Varying J/t modifies the width of the different phases as proposed in FIG. 19. Lastly, we note that $\delta = 1/4$ corresponds to the end of the plateau both for $J/t = 0.35$ and $J/t = 0.5$. Furthermore, the magnetization curves are strongly modified with $\delta > 1/4$ (data not shown) which suggests that this hole density corresponds to a singular point.

2. Charge gaps and exceeding of the Pauli limit

To study the charge degree of freedom of the system, we computed the two-particle gap Δ_{2p} (related to the inverse compressibility) and pairing energy Δ_p as a function of the magnetization m to discuss the nature of the ground state. With n_h the number of holes and S^z the total spin along the magnetic field, we have the definitions

$$\Delta_{2p}(S^z) = E(n_h + 2, S^z) + E(n_h - 2, S^z) - 2E(n_h, S^z), \quad (32)$$

and

$$\Delta_p(S^z) = E(n_h - 1, S^z + 1/2) + E(n_h - 1, S^z - 1/2) - E(n_h, S^z) - E(n_h - 2, S^z). \quad (33)$$

The evolution of these gaps under increasing magnetization is displayed on FIG. 18. Superconducting correlations

are also algebraic when the pairing energy is finite from FIG. 6 of Ref. [21]. These two observations confirm that the system is in a superconducting state, except in the $m = \delta$ plateau where a finite two-particle charge gap is found as well as a strong reduction of all superconducting correlations from FIG. 6 of Ref. [21]. However, the field ϕ_{\downarrow}^+ remains gapless in the irrational plateau while other fields are gapful. This suggests that the system is in a metallic phase in this plateau phase. Increasing the magnetic field brings the system back into a superconducting phase, giving an example of reentrant superconductivity which shares similarity with a proposal for a bilayer system⁴¹. The finite value of Δ_{2p} in the thermodynamic limit within the plateau phase can be inferred by using Eq. (32) and the constraint $m = \delta$ for continuous values of hole doping, which are more general hypothesis than the particular case under study. Indeed, it is straightforward to find that it exactly equals the width $E(n_h, S^z + 1) - E(n_h, S^z - 1)$ of the plateau in the thermodynamical limit. This is coherent with the numerical results of FIG. 18 obtained at fixed δ . It simply means that removing a hole pair in a system which has $m = \delta$ (i.e. the same number of hole pairs and magnons) is energetically equivalent to adding a magnon in a system with $m' = \delta'$ at a slightly lower density. Thus, one has to pay the energy gap of the $m' = \delta'$ plateau for that, and this gap equals the $m = \delta$ gap in the thermodynamical limit.

We now come to the computation of the Pauli limit H_p and of the superconducting critical field H_c . We have access numerically to the condensation energy of a pair of electrons through $\Delta_p(S^z = 0)$. Since paired electrons are paired in a singlet state, they are not stabilized by the Zeeman effect contrary to two free electrons that are stabilized by $-2 \times \frac{1}{2} \times H$. Equaling these two energies gives the simple relation for the Pauli field $H_p = \Delta_p(S^z = 0)$. The critical field is deduced from the location at which $\Delta_p(S^z)$ crosses zero which gives a critical magnetization m_c and in turn the critical field H_c reported on FIG. 17. It is important to note that this calculations are direct and without approximations. The superconducting critical field H_c can also be interpreted in the bosonization language as the emptying of the (π, \downarrow) band (see Sec. IV C). From FIG. 17 and FIG. 19, it is clear that Pauli limit is exceeded at low doping and for a wide region of parameters. This exceeding can be explained via the FFLO mechanism as discussed in Sec. IV D from the behavior of the superconducting correlations.

At last, we remark from FIG. 18 that the pairing energy has a discontinuity upon magnetizing the ladder (in the $m \rightarrow 0$ limit) very similar to the known discontinuity of the spin gap^{42,43} upon doping the ladder (in the $\delta \rightarrow 0$ limit). Note also that the strong reduction of the pairing energy and of the spin gap for $\delta = 1/4$ observed on FIG. 17 is related to the proximity of the CDW phase¹⁴ which occurs for $J/t \sim 0.2$.

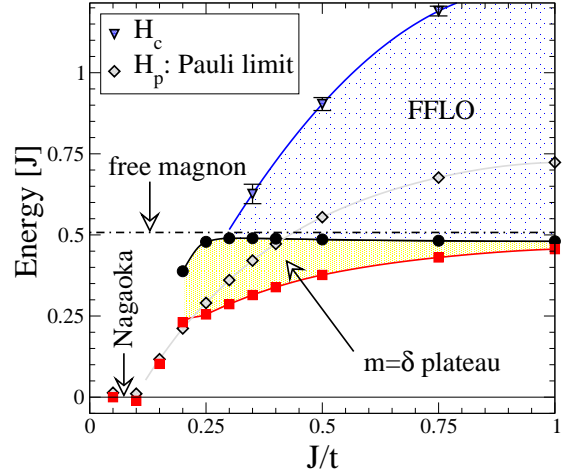


FIG. 19: (Color online) H_c , H_p and $m = \delta$ plateau on an isotropic two-leg t-J ladder doped with 2 holes as a function of J/t (this corresponds to the $\delta \rightarrow 0$ limit of the phase diagram of FIG. 17). The red curve (squares) corresponds to the upper limit of the $m = 0$ plateau and the lower limit of the $m = \delta$ plateau while the black curve (circles) to the upper limit of the $m = \delta$ plateau. The FFLO phase is delimited by the black curve (circles) and the blue curve (triangles). Results are extrapolated from DMRG results on systems with $L = 32, 48, 64$. For small J/t , a Nagaoka phase is found but because of strong finite size effects, we do not discuss this part of the diagram. Lines are guide to the eyes.

3. Phase diagram

The phase diagram of FIG. 17 is proposed to be generic in the coupled band regime for strong repulsive interactions. In addition to the magnetic properties described above, the system is in a LE superconducting state in the $m = 0$ plateau, in a Luttinger Liquid superconducting phase below H_c and in a metallic phase in the $m = \delta$ plateau phase. Above H_c , the system switches to a metallic phase with three ungapped sectors which couple both spin and charge degrees of freedom. The central charge c is expected to take the following values in each phase encountered as the magnetic field is increased (taking for example a vertical cut on FIG. 17 with $\delta = 0.063$): $c = 1$ ($m = 0$ plateau), 2 (FFLO below the $m = \delta$ plateau), 1 ($m = \delta$ plateau), 2 (FFLO above the $m = \delta$ plateau), 3 (above H_c), 2 (saturation phase). Note that one could expect a last transition $c = 2 \rightarrow 1$ for certain parameters, corresponding to a situation where the $(0, \uparrow)$ is completely filled. Since such a transition would induce a cusp in the magnetization curve and there is no sign of it on FIG. 16, we conclude that $c = 2$ is the value for the saturation in this regime.

To evaluate the role of J/t on this generic phase diagram, we computed various energy gaps and critical fields in the $\delta \rightarrow 0$ limit, i.e. for two holes on a ladder with $L \rightarrow \infty$. Results are extrapolated from systems of length $L = 32, 48, 64$ and are displayed on FIG. 19. First, we note that for J/t very small, a Nagaoka phase

competes the LE phase and induces strong finite size effects in the ground states, thus the displayed boundary between these phases *does not* correspond to the thermodynamical transition. Hence, we only focus on points for which the LE phase is stable (on finite size systems) which are found to be qualitatively for $0.25 \leq J/t \leq 1.0$. For large J/t the model undergoes a phase separation between holes and spins and we are not interested in the behavior near this instability. In this region of parameters, we have the following behavior: the width of the plateau increases for decreasing J/t (for $J/t = 1.0$, the $m = \delta$ plateau is hardly visible at finite density, data not shown), while the exceeding of the Pauli limit increases with J/t (which simply follows the increase of the pairing energy).

These elementary excitation gaps at $\delta \rightarrow 0^+$ can be related to the dynamics of the system⁴³ when $m = 0$. The difference between $\min(\Delta_p, \Delta_M)$ and the spin gap corresponds to the binding energy of the resonant magnetic mode. It is interesting to note that the upper limit of the $m = \delta$ plateau is approximatively independent of J/t and corresponds to a free magnon (which is nothing but the spin gap of the undoped system $\Delta_M \sim J/2$). Indeed, once the hole pair is bound to a magnon, the next magnetic excitation is to create a magnon in the remaining undoped background, which cost is Δ_M , slightly renormalized by the scattering with the holes-magnon bound-state. This supports the phenomenological mechanism proposed in Ref. [21] for the opening of the irrational plateau. The binding of the hole pair to the magnon comes from the gain in kinetic energy holes have in a locally ferromagnetic environment. It is thus expected that the binding energy increases with t/J . It is also likely to find such a bound state in the vicinity of a Nagaoka phase which here competes the LE phase. It also explains the decreasing of the pairing energies as J/t is reduced. Note that previous studies of this resonant magnetic mode with exact diagonalization⁴³ and periodic boundary conditions agree with these results, and hence suggest that open boundary conditions do not affect this generic phase diagram.

V. COUPLED CHAIN REGIME

A. Dominant exchange model

By strongly reducing the interchain hopping amplitude, one can reach the coupled chain regime in which interchain hopping is an irrelevant perturbation^{44,45,46,47} and the relevant interchain couplings are either the Josephson coupling (for attractive intrachain interactions) or the exchange coupling (for repulsive interchain interaction). An important point is that even if the bare model has only interchain hopping, Josephson and exchange couplings are generated by the Renormalization Group (RG) flow^{45,46,47} and, as a result, the effective model always contain this type of interactions. In the rest of the paper, we will call this strong coupling limit the “chain representation”. The bosonized Hamiltonian describing the two uncoupled chains reads³⁷:

$$\mathcal{H} = \sum_{\substack{i=1,2 \\ \nu=\rho,\sigma}} \int \frac{dx}{2\pi} \left[u_\nu K_\nu (\pi \Pi_{\nu,i})^2 + \frac{u_\nu}{K_\nu} (\partial_x \phi_{\nu,i})^2 \right], \quad (34)$$

where we have dropped terms $\propto g_{1\perp} \cos \sqrt{8} \phi_{\sigma,i}$ since these terms are marginally irrelevant in the case of repulsive interactions. In the case of attractive interactions, they also become irrelevant upon the application of a magnetic field strong enough to induce a C-IC transition³⁹.

1. Dominant exchange

For small $J_{\parallel}/t_{\parallel}$ ratios, the analysis of the scaling dimensions in the t-J model on a single chain⁴⁸ shows that the dominant interchain coupling is the exchange one. This term reads

$$\frac{2J_{\perp}\alpha}{(2\pi\alpha)^2} \cos \sqrt{2}(\phi_{\rho,1} - \phi_{\rho,2}) \left[\cos \sqrt{2}(\theta_{\sigma,1} - \theta_{\sigma,2}) + \frac{1}{2} \cos \sqrt{2}(\phi_{\sigma,1} - \phi_{\sigma,2}) + \frac{1}{2} \cos \sqrt{2}(\phi_{\sigma,1} + \phi_{\sigma,2} + 2\pi mx) \right], \quad (35)$$

where we have the usual definition $\theta_{\nu,i} = \int \pi \Pi_{\nu,i}$. For nonzero magnetization, the last term is oscillating and drops from the Hamiltonian. It is convenient to introduce the new fields

$$\begin{aligned} \phi_{\nu,\pm} &= \frac{1}{\sqrt{2}}(\phi_{\nu,1} \pm \phi_{\nu,2}), \\ \theta_{\nu,\pm} &= \frac{1}{\sqrt{2}}(\theta_{\nu,1} \pm \theta_{\nu,2}). \end{aligned}$$

With this transformation, the exchange term is rewritten as

$$\frac{2J_{\perp}}{(2\pi\alpha)^2} \int dx \cos 2\phi_{\rho-} \left[\cos 2\theta_{\sigma-} + \frac{1}{2} \cos 2\phi_{\sigma-} \right]. \quad (36)$$

Moreover, the two chains being equivalent, the chain Hamiltonian is rewritten as

$$\mathcal{H} = \sum_{\substack{r=\pm \\ \nu=\rho, \sigma}} \int \frac{dx}{2\pi} \left[u_\nu K_\nu (\pi \Pi_{\nu,r})^2 + \frac{u_\nu}{K_\nu} (\partial_x \phi_{\nu,r})^2 \right]. \quad (37)$$

Obviously, the Hamiltonians describing the fields $\phi_{\sigma+}$ and $\phi_{\rho+}$ are purely quadratic indicating that the total charge and the total spin excitations are gapless. The fields $\phi_{\sigma-}$ and $\phi_{\rho-}$ are described by a generalized sine Gordon model. The sine Gordon interaction term (36) can be treated within a RG analysis. The scaling dimensions of the term $\cos 2\phi_{\rho-} \cos 2\theta_{\sigma-}$ is $K_{\rho-} + K_{\sigma-}^{-1}$ and scaling dimensions of the term $\cos 2\phi_{\rho-} \cos 2\phi_{\sigma-}$ is $K_{\rho-} + K_{\sigma-}$. From the analysis of Ref. [28] we can conclude that in the case of interest we have $K_{\sigma-} > 1$ and $\cos 2\phi_{\rho-} \cos 2\theta_{\sigma-}$ is the most relevant term and for anti-ferromagnetic J_\perp the ground state has $\langle \phi_{\rho-} \rangle = 0 \pmod{\pi}$ and $\langle \theta_{\sigma-} \rangle = \frac{\pi}{2} \pmod{\pi}$.

2. Most divergent superconducting fluctuations

The expression of the intrachain order parameters in terms of the fields in (37) can be found in Ref. [37]. When re-expressed in terms of the \pm fields and denoting $q = \pi m$, the singlet operator reads:

$$\begin{aligned} O_{SS,i} &= \sum_{\sigma} \sigma e^{iq\sigma x} \psi_{R,i,\sigma} \psi_{L,i,-\sigma} \\ &\sim \sum_{\sigma} \sigma e^{iq\sigma x} e^{i(\theta_{\rho+} - (-)^i \theta_{\rho-})} e^{-i\sigma(\phi_{\sigma+} - (-)^i \phi_{\sigma-})}, \end{aligned} \quad (38)$$

and, for triplets operators, we have:

$$\begin{aligned} O_{TS,i,S^z=0} &= \sum_{\sigma} e^{iq\sigma x} \psi_{R,i,\sigma} \psi_{L,i,-\sigma} \\ &\sim \sum_{\sigma} e^{iq\sigma x} e^{i(\theta_{\rho+} - (-)^i \theta_{\rho-})} e^{-i\sigma(\phi_{\sigma+} - (-)^i \phi_{\sigma-})}, \\ O_{TS,i,S^z=1} &= \psi_{R,i,\uparrow} \psi_{L,i,\uparrow} \\ &\sim e^{i(\theta_{\rho+} - (-)^i \theta_{\rho-})} e^{-i(\theta_{\sigma+} - (-)^i \theta_{\sigma-})}. \end{aligned} \quad (39) \quad (40)$$

For the interchain operators, the singlet operator reads:

$$\begin{aligned} O'_{SS} &= \sum_{\sigma} \sigma e^{iq\sigma x} \psi_{R,1,\sigma} \psi_{L,2,-\sigma} \\ &\sim \sum_{\sigma} \sigma e^{iq\sigma x} e^{i[\theta_{\rho+} - \phi_{\rho-} + \sigma(\theta_{\sigma-} - \phi_{\sigma+})]}, \end{aligned} \quad (41)$$

while the triplet ones read:

$$\begin{aligned} O'_{TS,S^z=0} &= \sum_{\sigma} e^{iq\sigma x} \psi_{R,1,\sigma} \psi_{L,2,-\sigma} \\ &\sim \sum_{\sigma} e^{iq\sigma x} e^{i[\theta_{\rho+} - \phi_{\rho-} + \sigma(\theta_{\sigma-} - \phi_{\sigma+})]}, \end{aligned} \quad (42)$$

$$\begin{aligned} O'_{TS,S^z=1} &= \psi_{R,1,\uparrow} \psi_{L,2,\uparrow} \\ &\sim e^{i(\theta_{\rho+} - \phi_{\rho-} + \theta_{\sigma+} - \phi_{\sigma-})}. \end{aligned} \quad (43)$$

Since $\langle \phi_{\rho-} \rangle = 0$, we have $\langle e^{i\phi_{\rho-}} \rangle \neq 0$ and by duality $\langle e^{i\theta_{\rho-}(x)} e^{i\theta_{\rho-}(0)} \rangle \sim e^{-x/\xi_-}$. This property implies that all the intrachain superconducting correlations should decay exponentially along the chains. On the other hand, the interchain correlations are reinforced. The physical picture is that in this situation fermions of opposite spin on each chain are bound together by the exchange interaction. Whether the dominant superconductivity is the interchain one or the intrachain one depends on the value of $K_{\sigma-}$. Since we have $K_{\sigma-} > 1$ in our case, the dominant superconducting correlations are the interchain singlet and the interchain triplet $S^z = 0$. Note that these two operators have exactly the same critical exponents. In the case of dominant Josephson coupling, the situation is reversed.

3. $S^z = 1$ triplet with a $2k_F$ momentum

It is also straightforward to derive an expression of the operator $e^{2ik_{F,\sigma}x} \psi_{R,1,\sigma} \psi_{R,2,\sigma}$ associated to the $2k_F$ triplet correlations. This expression reads:

$$e^{2ik_{F,\sigma}x} e^{i(\theta_{\rho+} - \phi_{\rho+})} e^{i\sigma(\theta_{\sigma+} - \phi_{\sigma+})} \quad (44)$$

This expression again shows power law correlations with the critical exponent:

$$\frac{1}{2} (K_{\rho+} + K_{\rho+}^{-1} + K_{\sigma+} + K_{\sigma+}^{-1}) \quad (45)$$

very similar to what has been obtained in Sec. IV B 2.

B. favoring the Josephson coupling in the coupled chain regime

Let us consider the regime of small interchain hopping and assume that now the intra-chain terms are such that $J_\parallel \sim 4t_\parallel$. In this case, the dominant term becomes the Josephson coupling⁴⁸ and the perturbation term Eq. (36) is replaced by:

Dominant interaction	Dominant superconducting correlations	Critical exponent
Exchange coupling ($K_{\sigma-} > 1$)	rung singlet and rung triplet $S^z = 0$	$\frac{1}{2K_{\rho+}} + \frac{K_{\sigma+}}{2}$
Josephson coupling ($K_{\sigma-} > 1$)	leg triplet $S^z = 1$	$\frac{1}{2K_{\rho+}} + \frac{1}{2K_{\sigma+}}$

TABLE III: The different dominant superconducting fluctuations with the associated critical exponents. Josephson coupling dominates for $K_{\rho-} > 1$ and exchange coupling dominates for $K_{\rho-} < 1$.

$$\frac{2\lambda\alpha}{(2\pi\alpha)^2} \cos \sqrt{2}(\theta_{\rho,1} - \theta_{\rho,2}) \left[\cos \sqrt{2}(\theta_{\sigma,1} - \theta_{\sigma,2}) + \frac{1}{2} \cos \sqrt{2}(\phi_{\sigma,1} - \phi_{\sigma,2}) + \frac{1}{2} \cos \sqrt{2}(\phi_{\sigma,1} + \phi_{\sigma,2} + 2\pi mx) \right]. \quad (46)$$

The treatment parallels the one of the exchange coupling in Sec. V A 1. The Josephson term is rewritten in the form:

$$\frac{2\lambda}{(2\pi\alpha)^2} \int dx \cos 2\theta_{\rho-} \left[\cos 2\theta_{\sigma-} + \frac{1}{2} \cos 2\phi_{\sigma-} \right]. \quad (47)$$

The scaling dimensions of the term $\cos 2\theta_{\rho-} \cos 2\theta_{\sigma-}$ is $K_{\rho-}^{-1} + K_{\sigma-}^{-1}$ and scaling dimensions of the term $\cos 2\phi_{\rho-} \cos 2\phi_{\sigma-}$ is $K_{\rho-}^{-1} + K_{\sigma-}$. A similar RG analysis to the one of Sec. V A 1 yields for $K_{\sigma-} > 1$ $\langle \theta_{\rho-} \rangle = 0$ (mod π) and $\langle \theta_{\sigma-} \rangle = \frac{\pi}{2}$ (mod π) and for $K_{\sigma-} > 1$ $\langle \theta_{\rho-} \rangle = 0$ (mod π) and $\langle \phi_{\sigma-} \rangle = \frac{\pi}{2}$ (mod π). This time, interchain correlations are decaying exponentially, and the dominant superconducting correlations are the intrachain ones. Since $K_{\sigma-} > 1$, $\langle \theta_{\sigma-} \rangle = \frac{\pi}{2}$ and the intrachain $S^z = 1$ triplet superconductivity is dominant. For $K_{\sigma-} < 1$ the dominant superconducting correlations are the intrachain singlet and intrachain triplet $S^z = 0$.

The results are summarized in the table III where the critical exponents η_α are defined by $\langle O_\alpha(x)O_\alpha(0) \rangle \sim |x|^{-\eta_\alpha}$. We note that triplet $S^z = 1$ superconducting correlations can never coexist with singlet superconducting correlations.

We have tried to observe these predictions numerically but using both the t-J model with small t_\perp, J_\perp and Hubbard model with small t_\perp . Unfortunately, for large J_\parallel/t_\parallel , the system with open boundary conditions has edge effects due to the proximity of the phase separation which occurs generically in the t-J model for large J/t . When edge effects are absent and in the Hubbard model, we did not find evidences of the proposed predictions, i.e. we mostly found cases related to the coupled bands regime fixed point. Still, contrary to the isotropic case which has been widely studied numerically at zero magnetization, a systematic study of the phase diagram at zero magnetization would be necessary before tackling the system under magnetic field. This systematic study is out of the scope of the present article.

VI. CONCLUSION

In conclusion, we studied the case of two fermionic coupled chains, or ladders, under a magnetic field inducing a Zeeman effect in the system. The first situation we addressed was the free and strong-coupling limits. We found that large doping-dependent magnetization plateaus occur for “coupled-dimers” systems (with large interactions on the rungs) and that pairing is not expected in the $m = \delta$ magnetization plateau phase. For a system with isotropic couplings, we showed that $m = \delta$ plateaus also exist and but pairing survives to much higher magnetizations. Furthermore, the computation of the one and two-particles gap and bosonization interpretation proved that the plateau phase is metallic while the system is in a superconducting state below and above this plateau. In addition, we computed the superconducting upper critical field which is much larger than the Pauli limit for a wide range of the parameters of the t-J model. Superconducting correlation functions precisely agree with the bosonization predictions up to the accuracy of our methods. Turning to the coupled-chain regime, other interesting unconventional behaviors are predicted for the superconducting correlations with, for instance, the possibility of having polarized triplet correlations under high magnetic fields. However, quick numerical investigations study were not able to find good parameters providing evidences of such predictions.

Discussion on experiments – We now briefly discuss consequences for experiments. First of all, the possibility of measuring irrational magnetization plateau would give a direct access to the hole doping δ . However, the magnetization is a global measurement summing up to the contribution of all subsystems. For instance, the magnetization curve of SCCO has very recently been measured⁴⁹ but the main contribution comes from the chains subsystem. On the other hand, local measurements such as NMR under high magnetic field would only give the signal corresponding to the ladder subsystem.

The superconducting critical field $H_c(T)$ of SCCO has been measured under high pressure^{18,19} and displays a strong anisotropy and anomaly in the $H_c(T)$ curvature (diverging as $T \rightarrow 0$). Furthermore, $H_c(T)$ much larger

than standard Pauli limit are found, suggesting an exceeding of the latest. The nature of the superconductivity in SC CO is a long-standing debate because of its complex structure and the requirement of high pressure experiments. Questions such as the nature of the pairing or the dimensionality of superconductivity have not reached full agreement yet. One possibility is that superconducting fluctuations of the RVB type develops in the ladder subsystem leading to superconductivity when these ladders are coupled through Josephson coupling (T_c being controlled by this coupling rather than by the magnetic energy scale J). In this case our study suggests that the FFLO mechanism appears on the ladder subsystem which could be stabilized when ladders are coupled. The other possibility would be that the superconducting

phase is really two-dimensional⁵⁰, requiring other explanations of the exceeding of Pauli limit such as triplet pairing¹⁹ when $H=0$. NMR measurements⁵¹ also showed that superconductivity survives under rather high field but p -wave superconductivity was proposed here.

Acknowledgments

G.R. would like to thank IDRIS (Orsay, France) and CALMIP (Toulouse, France) for use of supercomputer facilities. G. R., P. P. and D. P. thank Agence Nationale de la Recherche (France) for support.

* Electronic address: roux@irsamc.ups-tlse.fr
 † Electronic address: Edmond.Orignac@ens-lyon.fr

¹ P. Fulde and R. A. Ferrell, Phys. Rev. **135**, A550 (1964); A. I. Larkin and Y. N. Ovchinnikov, Sov. Phys. JETP **20**, 762 (1965); R. Casalbuoni and G. Nardulli, Rev. Mod. Phys. **76**, 263 (2004).

² T. Ishiguro in *High Magnetic Fields*, vol. 595 of *Lecture notes in physics* (Springer, 2002).

³ M. Sigrist, AIP Conf. Proc. **789**, 165 (2005).

⁴ E. Dagotto and T. M. Rice, Science **271**, 618 (1996); T. M. Rice, Z. Phys. B **103**, 165 (1997); E. Dagotto, Rep. Prog. Phys. **62**, 1525 (1999).

⁵ D. C. Cabra, A. Honecker, and P. Pujol, Phys. Rev. Lett. **79**, 5126 (1997); Phys. Rev. B **58**, 6241 (1998).

⁶ G. Chaboussant *et al.*, Phys. Rev. Lett. **79**, 925 (1997); Phys. Rev. Lett. **80**, 2713 (1998).

⁷ B. C. Watson *et al.*, Phys. Rev. Lett. **86**, 5168 (2001).

⁸ C. P. Landee, M. M. Turnbull, C. Galeriu, J. Giantsidis, and F. M. Woodward, Phys. Rev. B **63**, 100402(R) (2001).

⁹ H. Frahm and C. Sobiella, Phys. Rev. Lett. **83**, 5579 (1999).

¹⁰ D. C. Cabra, A. De Martino, A. Honecker, P. Pujol, and P. Simon, Phys. Lett. A **268**, 418 (2000).

¹¹ D. C. Cabra, A. De Martino, A. Honecker, P. Pujol, and P. Simon, Phys. Rev. B **63**, 094406 (2001).

¹² E. Orignac and D. Poilblanc, Phys. Rev. B **68**, 052504 (2003); D. Poilblanc, D. J. Scalapino and S. Capponi, Phys. Rev. Lett. **91**, 137203 (2003); D. Poilblanc and D. J. Scalapino, Phys. Rev. B **71**, 174403 (2005);

¹³ C. A. Hayward, D. Poilblanc, R. M. Noack, D. J. Scalapino, and W. Hanke, Phys. Rev. Lett. **75**, 926 (1995).

¹⁴ S. R. White, I. Affleck, and D. J. Scalapino, Phys. Rev. B **65**, 165122 (2002).

¹⁵ P. W. Anderson, Science **235**, 1196 (1987).

¹⁶ A. Gozar and G. Blumberg, *Frontiers in Magnetic Materials* (Springer-Verlag, 2005), pp. 653-695.

¹⁷ M. Uehara, T. Nagata, J. Akimitsu, H. Takahashi, N. Mori, and K. Kinoshita, J. Phys. Soc. Jpn. **65**, 2764 (1996); D. Jerome, P. Auban-Senzier, and Y. Piskunov in *High Magnetic Fields*, vol. 595 of *Lecture notes in physics* (Springer, 2002).

¹⁸ D. Braithwaite, T. Nagata, I. Sheikin, H. Fujino, J. Akimitsu, and J. Flouquet, Solid State Com. **114**, 533 (2000).

¹⁹ T. Nakanishi, N. Motoyama, H. Mitamura, N. Takeshita, H. Takahashi, H. Eisaki, S. Uchida, and N. Mori, Phys. Rev. B **72**, 054520 (2005).

²⁰ M. Matsukawa, Y. Yamada, M. Chiba, H. Ogasawara, T. Shibata, A. Matsushita, and Y. Takano, Physica C **411**, 101 (2004); S. Sasaki, S. Watanabe, Y. Yamada, F. Ishikawa, K. Fukuda, and S. Sekiya (2006), cond-mat/0603067.

²¹ G. Roux, S. R. White, S. Capponi, and D. Poilblanc, Phys. Rev. Lett. **97**, 087207 (2006).

²² S. R. White, Phys. Rev. Lett. **69**, 2863 (1992); Phys. Rev. B **48**, 10345 (1993).

²³ U. Schollwöck, Rev. Mod. Phys. **77**, 259 (2005).

²⁴ D. C. Cabra, A. De Martino, P. Pujol, and P. Simon, Europhys. Lett. **57**, 402 (2002).

²⁵ T. Pruschke and H. Shiba, Phys. Rev. B **46**, 356 (1992).

²⁶ K. Yang, Phys. Rev. B **63**, 140511(R) (2001).

²⁷ M. Yamanaka, M. Oshikawa, and I. Affleck, Phys. Rev. Lett. **79**, 1110 (1997); M. Oshikawa, M. Yamanaka, and I. Affleck, Phys. Rev. Lett. **78**, 1984 (1997); P. Gagliardini, S. Haas, and T. M. Rice, Phys. Rev. B **58**, 9603 (1998).

²⁸ N. Nagaosa, Sol. State Comm. **94**, 495 (1995); N. Nagaosa and M. Oshikawa, J. Phys. Soc. Jpn. **65**, 2241 (1996).

²⁹ D. V. Khveshchenko and T. M. Rice, Phys. Rev. B **50**, 252 (1994).

³⁰ A. M. Finkelstein and A. I. Larkin, Phys. Rev. B **47**, 10461 (1993).

³¹ H. J. Schulz, Phys. Rev. B **53**, R2959 (1996).

³² L. Balents and M. P. A. Fisher, Phys. Rev. B **53**, 12133 (1996).

³³ M. Troyer, H. Tsunetsugu, and T. M. Rice, Phys. Rev. B **53**, 251 (1996).

³⁴ M. Fabrizio, Phys. Rev. B **48**, 15838 (1993).

³⁵ H. Frahm and V. E. Korepin, Phys. Rev. B **42**, 10553 (1990); Phys. Rev. B **43**, 5653 (1991).

³⁶ E. Orignac and Y. Suzumura, Eur. Phys. J. B **23**, 57 (2001).

³⁷ T. Giamarchi, *Quantum Physics in one Dimension*, vol. 121 of *International series of monographs on physics* (Oxford University Press, Oxford, UK, 2004).

³⁸ S. R. White, Phys. Rev. B **72**, 180403(R) (2005).

³⁹ G. I. Dzhaparidze and A. A. Nersesyan, JETP Lett. **27**, 334 (1978); V. L. Pokrovsky and A. L. Talapov, Phys. Rev.

Lett. **42**, 65 (1979); H. J. Schulz, Phys. Rev. B **22**, 5274 (1980).

⁴⁰ E. Jeckelmann, D. J. Scalapino, and S. R. White, Phys. Rev. B **58**, 9492 (1998).

⁴¹ A. Buzdin, S. Tollis, and J. Cayssol, Phys. Rev. Lett. **95**, 167003 (2005).

⁴² H. H. Lin, L. Balents, and M. P. A. Fisher, Phys. Rev. B **58**, 1794 (1998).

⁴³ D. Poilblanc, O. Chiappa, J. Riera, S. R. White, and D. J. Scalapino, Phys. Rev. B **62**, 14633 (2000); D. Poilblanc, E. Orignac, S. R. White, and S. Capponi, Phys. Rev. B **69**, 220406(R) (2004).

⁴⁴ X. G. Wen, Phys. Rev. B **42**, 6623 (1990).

⁴⁵ D. Boies, C. Bourbonnais, and A.-M. S. Tremblay, in *Proceedings of the XXXIst Rencontres de Moriond*, edited by T. Martin, G. Montambaux, and J. Tran Thanh Van (Éditions Frontières, Gif sur Yvette, France, 1996).

⁴⁶ V. M. Yakovenko, JETP Lett. **56**, 510 (1992).

⁴⁷ S. Brazovskii and V. Yakovenko, J. de Phys. (Paris) Lett. **46**, L111 (1985).

⁴⁸ M. Ogata, M. U. Luchini, S. Sorella, and F. F. Assaad, Phys. Rev. Lett. **66**, 2388 (1991).

⁴⁹ R. Klingeler *et al.*, Phys. Rev. B **72**, 184406 (2005); Phys. Rev. B **73**, 014426 (2006).

⁵⁰ T. Nagata, M. Uehara, J. Goto, J. Akimitsu, N. Motoyama, H. Eisaki, S. Uchida, H. Takahashi, T. Nakanishi, and N. Môri, Phys. Rev. Lett. **81**, 1090 (1998).

⁵¹ N. Fujiwara, N. Môri, Y. Uwatoko, T. Matsumoto, N. Motoyama, and S. Uchida, Phys. Rev. Lett. **90**, 137001 (2003); J. of Phys.: Condens. Matter **17**, S929 (2005).